



HAL
open science

Prolonged trachyte storage and unusual remobilization at Piton de la Fournaise, La Réunion Island, Indian Ocean: Li, O, Sr, Nd, Pb and Th Isotope study

Ivan Vlastélic, Patrick Bachèlery, Olgeir Sigmarsson, Kenneth T. Koga, Estelle F. Rose-Koga, I Bindeman, Abdelmouhcine Gannoun, Jean-Luc Devidal, G Falco, T Staudacher

► To cite this version:

Ivan Vlastélic, Patrick Bachèlery, Olgeir Sigmarsson, Kenneth T. Koga, Estelle F. Rose-Koga, et al.. Prolonged trachyte storage and unusual remobilization at Piton de la Fournaise, La Réunion Island, Indian Ocean: Li, O, Sr, Nd, Pb and Th Isotope study. *Journal of Petrology*, 2021, 10.1093/petrology/egab048 . hal-03267101

HAL Id: hal-03267101

<https://uca.hal.science/hal-03267101>

Submitted on 22 Jun 2021

HAL is a multi-disciplinary open access archive for the deposit and dissemination of scientific research documents, whether they are published or not. The documents may come from teaching and research institutions in France or abroad, or from public or private research centers.

L'archive ouverte pluridisciplinaire **HAL**, est destinée au dépôt et à la diffusion de documents scientifiques de niveau recherche, publiés ou non, émanant des établissements d'enseignement et de recherche français ou étrangers, des laboratoires publics ou privés.

1
2
3
4 1 **Prolonged trachyte storage and unusual remobilization at Piton de**
5
6 2 **la Fournaise, La Réunion Island, Indian Ocean: Li, O, Sr, Nd, Pb and**
7
8 3 **Th Isotope study**
9
10
11 4

12
13 5 Running title: Exhuming old trachyte, La Réunion Island
14
15 6
16
17 7
18
19 8
20
21 9

22
23 10 I. Vlastelic^(1*), P. Bachèlery⁽¹⁾, O. Sigmarsson^(1,2), K.T. Koga⁽¹⁾, E.R. Rose-Koga⁽¹⁾, I. Bindeman⁽³⁾,
24 11 A. Gannoun⁽¹⁾, J.-L. Devidal⁽¹⁾, G. Falco⁽¹⁾, T. Staudacher⁽⁴⁾
25
26 12

27
28 13 ¹ Université Clermont Auvergne, CNRS, IRD, OPGC, Laboratoire Magmas et Volcans, F-63000
29 14 Clermont-Ferrand, France
30
31 15

32 16 ² Nordic Volcanological Center, Institute of Earth Sciences, University of Iceland, Reykjavík,
33 17 Iceland
34
35 18

36 19 ³ University of Oregon, Department of Geological Sciences, Eugene, OR 97403-1272, USA
37
38 20

39 21 ⁴ Observatoire Volcanologique du Piton de la Fournaise (OVPF), Institut de Physique du Globe
40 22 de Paris (IPGP), Sorbonne Paris-Cite, UMR 7154 CNRS, Université Paris Diderot, Bourg
41 23 Murat, France
42
43 24

44 25
45 26 * Corresponding author

46 27 email address: ivan.vlastelic@uca.fr

47 28 Phone : + 33 4 73 34 67 10
48
49
50
51
52
53
54
55
56
57
58
59
60

1
2
3 **Abstract**
4
5
6

7 31 La Réunion Island includes two major volcanic systems. About 0.5 Ma ago, Piton des Neiges
8 32 volcano declined, while Piton de la Fournaise volcano grew on its flank. Since then the Piton
9 33 de la Fournaise shield volcano has produced homogeneous lavas with chemical compositions
10 34 transitional between alkali and tholeiitic basalts. In April 2007, the volcano emitted a very
11 35 small volume of trachytic pumice during its largest historical eruption. We conducted a
12 36 comprehensive petrological and geochemical study of the pumice to understand the
13 37 occurrence of such silicic melt in the feeding system of this highly active basaltic volcano.
14 38 Isotopes of Sr, Nd, Pb and O, together with trace elements, indicate that the trachyte is
15 39 genetically related to the La Réunion mantle plume and derives from crystallization of a typical
16 40 basalt. The trachyte chemistry records a long and complex history of differentiation and
17 41 outgassing. The extensive depletion of moderately volatile elements (F, Cl, B, Cs, Cu, Li) and
18 42 less volatile uranium are consistent with exsolution of dense fluids at depths of several
19 43 kilometres. Lithium isotopes point to closed-system degassing during the very late stages of
20 44 crystallization. U-series isotopes and radiogenic $^{208}\text{Pb}^*/^{206}\text{Pb}^*$ constrain the time elapsed since
21 45 U loss to between 0.4 and 2.1 Ma. This age is as old or older than Piton de la Fournaise shield
22 46 edifice. The 2007 trachyte could thus be a liquid remnant of an extinct volcano, such as Piton
23 47 des Neiges or Les Alizés (Piton de la Fournaise proto-volcano). It could also result from partial
24 48 melting of an old syenite intrusion or remobilization of interstitial melts not fully solidified.
25 49 Thermal modelling indicates that the sustained heat flux from hot basaltic magmas rising from
26 50 the mantle can maintain temperatures above 800°C in the central feeding system, and prevent
27 51 magmas trapped in this hot core from total solidification.
28
29
30
31
32
33
34
35
36
37
38
39
40
41
42
43
44
45
46

47 53 Key words: Trachyte; Magma degassing; Li isotopes; U-series; La Réunion
48
49
50
51
52
53
54
55
56
57
58
59
60

INTRODUCTION

Volcanoes from intraplate ocean islands produce basalts during their shield building stage. More differentiated lavas are typically restricted to the declining and post-shield stages as the rate of mantle melt supply decreases (Macdonald & Katsura, 1964; Upton & Wadsworth, 1966, 1972; Moore et al., 2011). Yet, many basaltic shield volcanoes, such as those located on the islands of La Réunion, Hawaii, or Canary, occasionally produce small volumes of lava far more differentiated than basalts. In most cases, these compositions might be related to small-scale segregation of silicic liquids (up to 80 wt.% SiO₂) during crystallization of thick basaltic lava flows or lakes (Upton & Wadsworth, 1971; Helz, 2008; Martin & Sigmarsson, 2007). However, there is evidence that extensive differentiation also affects isolated magma lenses at depth. On the island of Hawaii, drilling of the Kilauea Lower East Rift Zone in 2005 encountered a melt of dacitic composition at 2488 m depth (Teplow et al., 2009). Andesite lava erupted along the same rift in 2018 (Gansecki & Lee, 2018; Gansecki et al., 2019). In the Canary archipelago, the October 2011 submarine eruption off El Hierro Island produced a small volume of rhyolitic magma (Sigmarsson et al., 2013). On La Réunion Island, the Piton de la Fournaise volcano produced a small volume of trachytic pumice during its largest historical eruption in April 2007 (Salaün et al., 2010). The occurrence of silicic melts in the plumbing system of basaltic volcanoes raises several questions related to (1) the source of the silicic melts and their genetic link with the basalts, (2) the depth, conditions and time-scales of magma storage, and (3) the degassing-crystallization history. Although the silicic melts are generally thought to originate from isolated pockets of highly evolved magma, it is unclear how such magma pockets can remain isolated within the plumbing system of highly active basaltic volcanoes regularly fed by mantle melts. The contribution of evolved melts to the compositional variability of basalts is suspected in some cases (Salaün et al. 2010), but remains difficult to distinguish from source heterogeneity.

The eruption of trachytic melt at Piton de la Fournaise is particularly puzzling because this volcano has produced lavas with limited compositional variations since 0.4 Ma, with CaO/Al₂O₃ mostly in the range of 0.65-0.85 (Albarède et al. 1997). To constrain the origin of this anomalous melt, we conducted a comprehensive petrological and geochemical study including analyses of major-trace element concentrations, volatile elements (H, C, S), radiogenic (Sr, Nd, Pb) and stable (Li, O) isotopes, and Th-U radioactive disequilibria. A major

1
2
3 86 finding is that the trachyte parental melt is older than Piton de la Fournaise shield edifice, and
4
5 87 must pertain to an ancient volcano of La Réunion Island.
6
7 88

8 89 **GEOLOGICAL CONTEXT**

9 90 10 91 **La Réunion Island**

11 92
12 93 The island of La Réunion (Indian Ocean) is the present location of the hotspot that created the
13 94 Deccan traps 66 Ma ago. The La Réunion edifice started to grow ~7 Ma ago on a NW-SE
14 95 lithospheric fracture that has controlled the main volcano-tectonic features of the island and
15 96 its slightly elongated shape (60 x 40 km). The emergent part of the island comprises an extinct
16 97 volcano (Piton des Neiges) in the NW and a basaltic shield volcano (Piton de la Fournaise) in
17 98 the SE (Fig. 1a). Piton des Neiges produced olivine basalts between 2.1 and 0.43 Ma ago, and
18 99 increasingly differentiated lavas (hawaiite, benmoreite, mugearite and trachyte) until its final
19 100 activity between 29 and 12 ka ago (Upton & Wadsworth, 1972; Gillot & Nativel, 1982; Deniel
20 101 et al., 1992). According to most recent works (Smietana, 2011; Lénat et al., 2012; Valer et al.,
21 102 2017a), Piton de la Fournaise started to grow 0.44 Ma ago on an ancient, now buried volcano
22 103 (named “Les Alizés”), whose last differentiated lavas (hawaiites and mugearites) outcrop at
23 104 the bottom of the Rivière des Remparts caldera (Fig. 1a). Between 0.44 Ma and 29 ka ago,
24 105 Piton des Neiges and Piton de la Fournaise were active simultaneously.
25 106
26 107

27 108 28 109 **Piton de la Fournaise volcano**

29 110 Four major collapses of Piton de la Fournaise volcano occurred 250, 150, 35 and 4.7 ka ago
30 111 (Gillot et al., 1994; Merle et al., 2010), resulting in concentric calderas. The volcano has
31 112 produced on average one eruption per year over the last three centuries, mostly inside the
32 113 most recent caldera, named the Enclos Fouqué (Fig. 1a) (Stieltjes & Moutou 1989; Villeneuve
33 114 & Bachèlery 2006). Piton de la Fournaise has a relatively simple plumbing system (Lénat et al.,
34 115 2012; Michon et al., 2016): The central magma path feeding summit eruptions produces
35 116 transitional basalts with restricted compositional variation ($5 < \text{MgO} < 8$ wt.%), often referred to
36 117 as Steady State Basalts (SSB) following Albarède et al. (1997). Magma erupted along the
37
38
39
40
41
42
43
44
45
46
47
48
49
50
51
52
53
54
55
56
57
58
59
60

1
2
3 118 peripheral system feeds rare eccentric eruptions, producing lava slightly enriched in MgO
4
5 119 (7.5–10 wt.%) and incompatible elements, and depleted in Ca relative to SSB (Famin et al.,
6
7 120 2009; Valer et al., 2017b). The main magma reservoir feeding both the central and peripheral
8
9 121 systems is thought to be located at a depth of about 7.5 km, 2-4 km west of the summit (Famin
10
11 122 et al., 2009; Peltier et al., 2009; Lénat et al., 2012). Temporal geochemical fluctuations
12
13 123 constrain the residence time of magmas in the main reservoir to between 10 and 30 years
14
15 124 (Albarède, 1993; Sigmarsson et al., 2005; Vlastélic & Pietruszka, 2016). All Piton de la
16
17 125 Fournaise lavas analysed so far have more than 5 wt.% MgO (Albarède et al., 1997), assuming
18
19 126 that the 400-530 ka old plagioclase-ultraphyric basalts collected at the bottom of the
20
21 127 Remparts caldera are late-stage products of the pre-existing Les Alizés volcano (Valer et al.,
22
23 128 2017a). The most differentiated lavas of the historical period have 5.8-6.1 wt.% MgO and seem
24
25 129 to correspond to magmas stored during the longest periods of inactivity (3 to 6 years) (Boivin
26
27 130 & Bachèlery, 2009; Coppola et al., 2017).
28
29 131

30 132 **THE APRIL 2007 ERUPTION AND THE TRACHYTIC PUMICES**

31 133
32 134 After nine years of high activity, Piton de la Fournaise erupted between April 2 and May 1
33
34 135 2007 along the South-east Rift zone, at 590 m elevation within the Enclos Fouqué caldera (Fig.
35
36 136 1a). The eruption produced $210 \times 10^6 \text{ m}^3$ of lava, the largest volume produced by an eruption
37
38 137 of this volcano in at least two centuries (Bachèlery et al, 2010; Staudacher et al., 2009; Derrien,
39
40 138 2019). Between April 5 and 7, the summit of the volcano collapsed, while lava effusion rate
41
42 139 transiently exceeded $200 \text{ m}^3/\text{s}$ (Coppola et al., 2009). These two synchronous events were
43
44 140 ascribed to the withdrawal of the shallow magma chamber (Staudacher et al., 2009). The
45
46 141 eruption produced aphyric basalt with 7.0-7.6 wt.% MgO from April 2 to 5, and olivine-rich
47
48 142 basalts subsequently (Di Muro et al., 2014).

49 143 When the site became accessible, in the early days of June 2007, white to grey pumices were
50
51 144 found to the North West of the main eruptive vent (Piton Tremblet) (Fig. 1b). The nearby tree
52
53 145 trunks, partially stripped of their bark and riddled with olivine crystals, were testament to the
54
55 146 blast of an explosion in the area. The pumices are a few centimetres in size and include dark
56
57 147 basaltic glass, either as very small drops interspersed within the pumice and/or as millimetre
58
59 148 thick coating (Fig. 1c). Early field works noted that the pumices become darker towards the
60
149 opening fracture, as their content in basaltic glass increases. The volume of pumice is

1
2
3 150 extremely small and unlikely to exceed a few cubic meters. During the following years, the
4
5 151 2007 pumice fallout was covered by younger lava flows. Such trachytic components might
6
7 152 have been erupted in the past, but have not been found or preserved in the geological record
8
9 153 due to their very minor volume.

10 154 Preliminary analyses (Falco, 2009) revealed that the pumices are trachytic in composition. To
11
12 155 date, no study has focused on these samples, but their compositions were reported in two
13
14 156 papers: Salaün et al. (2010) observed that the composition of the 2007 trachyte plots on the
15
16 157 dominant fractionation trend of Piton de la Fournaise basalts. The authors suggested that
17
18 158 trachytic melts form within rarely used eccentric magma paths and contaminate the basaltic
19
20 159 melts, causing their small compositional variations. Vlastelic et al. (2011) showed that the
21
22 160 pumice underwent extensive loss of water, halogens (Cl, F) and semi-volatile elements (Li, B
23
24 161 and Cs), which they attributed to low-pressure, vapor-saturated crystallization during
25
26 162 prolonged magma storage, or fluxing of vapours exsolved from deeper magma.

27 163

28 29 164 **SAMPLES AND METHODS**

30 165

31
32 166 About 200 centimetre-sized pumice chips were collected to the west ("PN" group) and to the
33
34 167 east ("PS" group) of the opening fracture (Fig. 1b). Within the PS fallout field, white pumices
35
36 168 with very low amount of basaltic glass were found to the North of Piton Tremblet, at the
37
38 169 border of the April 2007 lava flow (21°16'51"S – 55°46'29"E). They are referred to as sample
39
40 170 0704-TRA. A few chips from groups PN and PS were crushed and finely powdered in an agate
41
42 171 mortar (samples 0704-PS and 0704-PN) to measure bulk major-trace element concentrations
43
44 172 and Sr-Nd-Pb-Th-Li-O isotope compositions. One chip from the PN group (NPON) and two
45
46 173 chips from the PS group (SPON and 0704-TRA) were selected for in situ analyses (EPMA and
47
48 174 SIMS). Bulk and in situ analyses were also performed on the basaltic glass coating. In addition,
49
50 175 trace elements and Li-Th-Pb isotopes were measured on single grains, glass and magnetic
51
52 176 fractions from samples NPON, SPON and 0704-TRA. Analyses were performed at Laboratoire
53
54 177 Magmas et Volcans (LMV, Clermont-Ferrand, France), Centre de Recherches Pétrographiques
55
56 178 et Géochimiques (CRPG, Nancy, France), Ecole Normale Supérieure (ENS, Lyon, France), and
57
58 179 Stable Isotope Laboratory at the University of Oregon (Eugene, USA).

58 180

59 60 181 **Electron Microscopy**

1
2
3 182
4
5 183 Polished thin sections (samples SPON and NPON) and resin mount (sample 0704-TRA) were
6
7 184 surveyed by Scanning Electron Microscopy (JSM 5910LV, LMV) operating in Backscattered
8
9 185 Electron (BSE) imaging mode. The major element compositions were measured by Electron
10
11 186 Probe Microanalysis (Cameca SX 100, LMV) using a 15-kV accelerating voltage. Beam current
12
13 187 and spot size were 15-nA and 1 μm for minerals, and 8-nA and 20 μm for glass, respectively.
14
15 188 The counting times on peak and background were 10 s.

16 189 17 18 190 **Bulk major and trace elements** 19

20 191
21 192 The two powders 0704-PS and 0704-PN were analysed for bulk major and trace element
22
23 193 content. Millimetre-sized grains of the basaltic coating and sample 0704-TRA were analysed
24
25 194 for trace elements only. Major elements were quantified at LMV by ICP-AES (HORIBA-Jobin-
26
27 195 Yvon ULTIMA C) after alkali fusion and nitric acid dissolution, as described by Gurioli et al.
28
29 196 (2018). For trace elements, different dissolution procedures were used to measure both
30
31 197 elements occurring in very low amounts and/or prone to contamination and elements hosted
32
33 198 in resistant minerals: conventional HF-HNO₃ attack at 90°C in Savillex vials, HF-HNO₃ attack
34
35 199 between 120 and 250°C in Parr pressure vessels (4749 type), ammonium bifluoride (NH₄HF₂)
36
37 200 dissolution at 230°C in PTFE vials following the method described by Zhang et al. (2012), and
38
39 201 alkali fusion. Trace elements were measured on the Agilent 7500 ICP-MS of the LMV as
40
41 202 described in Gurioli et al. (2018), with the exception of samples dissolved by alkali fusion,
42
43 203 which were measured on a Thermo Elemental X7 ICP-MS at CRPG. Trace element
44
45 204 concentrations acquired at LMV were calibrated externally (every 4 samples) with the USGS
46
47 205 BHVO-2 standard dissolved as samples and using the recommended values of Chauvel et al.
48
49 206 (2011). The external reproducibility, inferred from repeated analysis of BHVO-2 as unknown
50
51 207 is 6% or lower except for Pb (15%) (Electronic Appendix 1). More information on sample
52
53 208 preparation and analysis is given in Vlastelic et al. (2013a).

54 210 **Bulk C, H, S content** 55

56 211
57
58 212 The concentrations of C, H and S of the powder samples 0704-PS and 0704-PN were measured
59
60 213 at LMV using a Flash 2000 CHNS-O elemental analyser from Thermo Fisher Scientific. One

1
2
3 214 milligram of powder and the same amount of V_2O_5 were precisely weighted in a tin capsule
4
5 215 using a microbalance, and introduced into the 950°C high-temperature reactor. The
6
7 216 combustion gases (CO_2 , H_2O and SO_2) were separated in the coupled chromatography column
8
9 217 and quantified by thermal conductivity. Cystine ($\text{C}_6\text{H}_{12}\text{NO}_4\text{S}_2$) was used for calibration. The 2σ
10 218 errors of H and C measurements are in range of 12-18 % and 4-8 %, respectively.
11

12 219

14 220 **Sr-Nd-Pb isotopes**

16 221

18 222 Three pumice samples (0704-PS, 0704-PN and 0704-TRA) and the basalt coating were analysed
19 223 at LMV for bulk Sr-Nd isotopes. These samples, as well as chips from samples S-PON (n=1), N-
20 224 PON (n=1) and 0704-TRA (n=6), were analysed for Pb isotopes. Samples (100 mg of powder or
21 225 5-10 mg grains) were dissolved with 5 ml of distilled 29M HF and 1 ml 14M HNO_3 , at 90°C in
22 226 Savillex vials for 24 hours. For chips, the same dissolution was used to measure Pb isotopes
23 227 and trace elements. Sr and Pb were separated using Eichrom Sr specific resin (Deniel & Pin,
24 228 2001). Light Rare Earth Elements were extracted from the residual fraction using Tru.Spec
25 229 resin, and Nd separated from the adjacent lanthanides using Ln.Spec resin (Pin & Zalduegui,
26 230 1997). Procedural blanks were < 0.03 ng for Pb, < 0.1 ng for Nd, and < 1 ng for Sr. These blanks
27 231 are insignificant compared to the amounts of Sr, Nd and Pb extracted from samples, which
28 232 are between 5×10^2 (Pb) and 2×10^4 (Sr) times larger. $^{87}\text{Sr}/^{86}\text{Sr}$ and $^{143}\text{Nd}/^{144}\text{Nd}$ were measured
29 233 on a Thermo Fisher Scientific Triton Thermal Ionization Mass Spectrometer (TIMS), and were
30 234 corrected for mass fractionation using $^{86}\text{Sr}/^{88}\text{Sr}=0.1194$ and $^{146}\text{Nd}/^{144}\text{Nd}=0.7219$, respectively.
31 235 Repeated measurement of the NBS SRM 987 and Ames standards during the course of the
32 236 study yielded $^{87}\text{Sr}/^{86}\text{Sr}=0.710243 \pm 9$ (2σ , n=20) and $^{143}\text{Nd}/^{144}\text{Nd}=0.511958 \pm 8$ (2σ , n=16),
33 237 respectively. Lead isotope compositions were measured on a Thermo Fisher Scientific
34 238 Neptune Plus MC-ICPMS coupled to an Aridus II desolvating nebulizer system. The Pb
35 239 instrumental mass fractionation was corrected during measurement by doping the Pb
36 240 solutions with the TI NBS997 standard. The NBS981 standard was measured between every
37 241 two samples to correct Pb ratios for instrumental drift and the slight difference in mass
38 242 fractionation between Pb and TI. Data were normalized to the NBS981 standard using the
39 243 values of Todt et al. (1996). Repeated analysis of the NBS981 standard every two samples
40 244 yielded typical intra-session 2σ reproducibility of 100, 120 and 140 ppm for $^{206}\text{Pb}/^{204}\text{Pb}$,
41 245 $^{207}\text{Pb}/^{204}\text{Pb}$ and $^{208}\text{Pb}/^{204}\text{Pb}$, respectively. The 2σ reproducibility of the $^{208}\text{Pb}^*/^{206}\text{Pb}^*$ ratio

1
2
3 246 (defined as $[(^{208}\text{Pb}/^{204}\text{Pb})_S - (^{208}\text{Pb}/^{204}\text{Pb})_{\text{CD}}] / [(^{206}\text{Pb}/^{204}\text{Pb})_S - (^{206}\text{Pb}/^{204}\text{Pb})_{\text{CD}}]$ where subscripts S
4 and CD refer to sample and Canyon Diablo meteorite, respectively) was better than 600 ppm.
5 247
6
7 248

8 249 **U-Th disequilibria**

9 250
10 251 The rock powders (0704-PS and 0704-PN), glass (S-PON, N-PON, 0704-TRA) and magnetic
11 252 (0704-TRA) fractions were analysed at LMV for Th isotopes. All samples were dissolved using
12 253 conventional HF-HNO₃ attack. For glass and magnetic fractions, Th isotopes and trace
13 254 elements were analysed on same dissolution. Thorium was extracted using TRU-Spec resin
14 255 and purified using AG1-X8 anionic resin, following Carpentier et al. (2015). The ²³⁰Th/²³²Th
15 256 ratios were measured in static double collection mode on the same Neptune MC-ICPMS as for
16 257 Pb isotopes. The small ²³⁰Th peak was measured on a secondary electron multiplier with
17 258 adjustable quadrupole potential (RPQ). An in-house standard solution (ThS1) was repeatedly
18 259 measured to correct for instrumental mass bias and faraday cup to secondary electron
19 260 multiplier relative gain. Contribution of the ²³²Th tailing on ²³⁰Th was corrected using an
20 261 exponential fit of the ²³²Th peak tail. Repeated analysis of Th Specpure and ThS1 standards
21 262 yielded (²³⁰Th/²³²Th) = 0.157±0.002 (2σ, n=15) and (²³⁰Th/²³²Th) = 1.022±0.003 (2σ, n=12),
22 263 respectively. The ²³⁸U/²³²Th ratios were measured by ICP-MS, with a precision of 6 % estimated
23 264 from the repeated analysis of BHVO-2 standard. The error on the ²³⁸U/²³²Th ratio does not
24 265 exceed the individual errors on U and Th concentrations due to the significant correlation of
25 266 ²³⁸U and ²³²Th errors during ICPMS analysis.
26
27 267

28 268 **Bulk O isotope composition**

29 269
30 270 Oxygen isotope compositions of samples 0704-PS and 0704-PN were analysed by laser
31 271 fluorination in the Stable Isotope Laboratory at the University of Oregon following the method
32 272 described by Bindeman et al. (2008). A 35W CO₂-laser was used, and rock powders were
33 273 reacted with purified BrF₅ to release oxygen. Gases were purified cryogenically using liquid N₂
34 274 and by using a Hg-diffusion pump to eliminate traces of F₂ gas formed by fluorination. Oxygen
35 275 was then converted to CO₂ by reaction with platinum-graphite, and the yields were measured
36 276 by a baratron gauge. Then the CO₂ was analysed on a Thermo Fisher scientific MAT 253 mass
37 277 spectrometer. Internal precision varied from 0.14 to 0.20 ‰ (2σ). The standards used with

1
2
3 278 these analyses include San Carlos olivine ($\delta^{18}\text{O} = 5.25 \text{ ‰}$), Gore Mt Garnet (UWG2, $\delta^{18}\text{O} = 5.80$
4 279 ‰ , Valley et al., 1995) and OUG University of Oregon Garnet ($\delta^{18}\text{O} = 6.52 \text{ ‰}$). The $\delta^{18}\text{O}$ of
5 280 standards varied between 0.01 and 0.14 ‰ over the course of the study, and were used to
6 281 correct for day-to-day variability and absolute oxygen isotope compositions on the SMOW
7 282 scale.

8

9 283

10 284 **Bulk Li isotope composition**

11

12 285

13 286 In addition to Li data previously reported by Vlastelic et al. (2011), six grains of sample 0704-
14 287 TRA and one grain of the basaltic coating (0704-PN-BAS) were analysed for bulk lithium
15 288 isotope composition. About 50 mg of powder was dissolved in a mixture of concentrated
16 289 HClO_4 (0.3 ml) and HF (1 ml). Following Vlastelic et al. (2009a), we used 0.5M HCl and AG50W-
17 290 X8 cationic resin to isolate Li in two steps. Lithium isotope compositions were measured on
18 291 the Nu Plasma 500 MC-ICPMS of ENS Lyon coupled to a Nu DSN desolvator. Mass
19 292 discrimination was monitored using IRMM-016, which was run between every sample
20 293 analysis. Each sample was measured at least twice. Repeated analysis of the USGS BHVO-2
21 294 standard yielded ${}^7\text{Li}/{}^6\text{Li} = +4.3\text{‰} \pm 0.4$ (2σ , $n=8$).

22

23 295

24 296 **Lithium isotopes analysis by SIMS**

25

26 297

27 298 In-situ Li isotope compositions were measured on a polished section of sample 0704-TRA using
28 299 the CRPG SIMS 1280 ion microprobe. The mass resolution was set to 2000 to separate ${}^6\text{Li}^1\text{H}$
29 300 from ${}^7\text{Li}$. The measurements were made in single-collection mode using the central electron
30 301 multiplier for mass 5.8 (for background), ${}^6\text{Li}$ and ${}^7\text{Li}$, and with counting times in each cycle of
31 302 3, 12 and 4 s, respectively. Repose time was set to 3 s, 1 s and 1 s, respectively. One
32 303 measurement consists of 20 cycles, with 40 s pre-sputtering and automatic centring of the
33 304 secondary beam in the field aperture and in the contrast aperture and no energy offset was
34 305 applied. A primary beam intensity of 8 nA was used to make the lithium isotope
35 306 measurements with 20-25 μm spot sizes. The count rates on ${}^6\text{Li}$ ranged between 10000
36 307 counts/s in the basaltic glass and 500 counts/s in the trachyte glass, resulting in a one sigma
37 308 counting statistic between $\pm 1 \text{ ‰}$ and $\pm 2.8 \text{ ‰}$ for ${}^7\text{Li}/{}^6\text{Li}$, respectively. The standards used were
38 309 in house CRPG standards (a synthetic enstatite ENST-B and a natural basaltic glass NZ-06-14

1
2
3 310 from the Nazca ridge) as well as MPI-DING glass standards (ML3B, T1G, GOR132, GOR128,
4
5 311 ALV2748). The external error of $\delta^7\text{Li}$, estimated from repeated analysis of one glass, is 3.7‰
6
7 312 (2σ). Based on calibration before and after a session, variations of instrumental fractionation
8
9 313 were within the external reproducibility.

10 314

11 315 **RESULTS**

12 316

13
14
15
16 317 Bulk analyses, including concentrations of major-trace elements and C-H-S, and Sr-Nd-Pb-Th-
17
18 318 O-Li isotope compositions are reported in Electronic Appendix 1. Microprobe analyses of glass
19
20 319 and minerals are reported in Electronic Appendix 2, while lithium isotope analyses by SIMS
21
22 320 are given in Electronic Appendix 3.

23 321

24 322 **Mineralogy and petrology of the pumices**

25 323

26
27
28
29 324 The pumices show a hyaline texture with glass and microlites of feldspar in the matrix (Fig. 2).
30
31 325 Their colour varies from white to medium grey. Inspection of thin sections indicates that the
32
33 326 pumices contain 80 to 90 vol.% vesicle. Vesicles, ranging in size from several millimetres to a
34
35 327 few micrometres, are rounded or elongated, isolated or coalescent, separated by very thin
36
37 328 glass walls (a few tens to a few hundred μm). Pumice fragments are often coated by a dark
38
39 329 basalt glass (Fig. 2c). The yellowish-brown glass locally invades the pumice as fine droplets or
40
41 330 thin films (Fig. 2a and c). Mixing between the two magmas is restricted to areas of a few tens
42
43 331 of micrometres (Fig. 2c and f). In the trachytic liquid, microlites of $<1\ \mu\text{m}$ to $10\ \mu\text{m}$ of Na-rich
44
45 332 alkali feldspar occur (anorthoclase, $\text{An}_{4-11}\text{Ab}_{67-77}\text{Or}_{13-25}$, see Fig. 2f and Electronic Appendix 2).
46
47 333 In areas where the trachytic and basaltic liquids mix, the glass has variable compositions,
48
49 334 depending on the relative proportions of the two liquids (Fig. 2d-f). Small crystals ($<100\ \mu\text{m}$)
50
51 335 of magnetite and dendritic microcrystals (ranging in size from a few to tens micrometres) of
52
53 336 plagioclase (labradorite, $\text{An}_{49-62}\text{Ab}_{37-49}\text{Or}_{1-2}$, Electronic Appendix 2) are present. The mixed
54
55 337 glass also contains clinopyroxene crystals ($\text{En}_{33}\text{Fs}_{23}\text{Wo}_{44}$) with higher iron content than
56
57 338 clinopyroxenes occurring in basalts (Falco, 2009). Other mineral phases, such as olivine, when
58
59 339 present, are associated with the basaltic liquid. Pumice whole rock compositions and glass
60
340 mainly plot in the trachyte field of the total alkali versus silica diagram, whereas yellowish-
341 brown glasses are basalts (Fig. 3).

1
2
3 3424
5 343 **Bulk trace element contents**6
7 344

8 345 Trace element patterns normalized to the average composition of common La Réunion basalts
9 346 (referred to as steady state basalts) are shown on Figure 4 for the trachyte pumice and the
10 347 basalt glass. The trachyte pattern is complex: Nb, Ta, Be and rare earth elements lighter than
11 348 Eu define an enriched pattern, with normalized concentrations ranging from 2.1 for Sm up to
12 349 7.8 for Nb in sample 0704-TRA. Zirconium and Hf show positive anomalies, with Zr/Zr^*
13 350 ($Zr_N/(Sm_N \times Gd_N)^{0.5}$) ranging between 1.6 (0704-PN) and 3.0 (0704-TRA). Conversely, Cs, Cu, Li,
14 351 B, Pb, Eu, Sr, Ba and U show negative anomalies. Lithium and Cs show the strongest anomalies,
15 352 with Li/Li^* ($Li_N/(Tm_N \times Yb_N)^{0.5}$) as low as 0.02 in sample 0704-TRA. The increasing recovery of Zr,
16 353 Hf and heavy rare earth elements with dissolution strength (Electronic Appendix 4) indicates
17 354 that the pumice contains zircon, and constrains its modal abundance to between 0.06 (0704-
18 355 PN) and 0.16 wt.% (0704-TRA). The pumice samples generally have low compatible element
19 356 contents (e.g., Ni <40 ppm), with the exception of chip#5 of sample 0704-TRA that obviously
20 357 hosts some basalt (Electronic Appendix 1). The basalt pattern is flat, with incompatible
21 358 element concentrations ranging between 0.53 and 0.57 times those of steady state basalts,
22 359 due to the occurrence of ca. 50% cumulative olivine (Fig. 4). This characteristic is typical of
23 360 April 2007 basalts erupted after April 5 (Di Muro et al., 2014). Only lithium shows a slight
24 361 positive anomaly ($Li/Li^*=1.2$). The homogeneous depletion of incompatible elements and the
25 362 high Ni content of the basalt (887-1010 ppm, Electronic Appendix 1) are consistent with the
26 363 occurrence of cumulative olivine.

27 364

28 365 **Bulk content of C, H and S**

29 366

30 367 The samples 0704-PS and 0704-PN have between 487 and 727 ppm H, and between 373 and
31 368 970 ppm C (Electronic Appendix 1). The H content corresponds to 0.44-0.65 wt.% H₂O, which
32 369 is higher than the value of 0.2±0.1 wt.% previously determined on the glass by Raman
33 370 spectroscopy (Vlastelic et al., 2011). The C content corresponds to 0.14-0.36 wt.% CO₂. Sulphur
34 371 content is below the detection limit of 50 ppm for both samples.

35 372

36 373 **Sr-Nd-Pb isotopic composition**

1
2
3 374
4
5 375 The pumice samples show small variations of $^{206}\text{Pb}/^{204}\text{Pb}$ (18.897-18.943), $^{207}\text{Pb}/^{204}\text{Pb}$ (15.584-
6 376 15.596) and $^{208}\text{Pb}/^{204}\text{Pb}$ (38.979-39.027), a narrow range of $^{87}\text{Sr}/^{86}\text{Sr}$ (0.704213-0.704297), and
7 377 constant ϵNd (4.35 ± 0.12 (2σ)) (Electronic Appendix 1). These compositions plot well within
8
9 378 the Sr-Nd-Pb isotope field of La Réunion Island lavas (Fig. 5), but show slightly higher $^{87}\text{Sr}/^{86}\text{Sr}$
10 379 at given ϵNd than Piton de la Fournaise historic lavas (Fig. 5a). The basalt coating plots within
11 380 the field of the April 2007 eruption in Sr-Nd and Pb-Pb isotope spaces. It has a relatively
12 381 unradiogenic Pb signature ($^{206}\text{Pb}/^{204}\text{Pb}$ of 18.873, Fig. 5b) that characterizes the lavas emitted
13 382 during the eruption paroxysm on April 5 (Vlastelic et al., 2009b).
14
15
16
17
18
19
20
21

22 384 ^{230}Th - ^{238}U disequilibria

23 385
24
25 386 Thorium isotope compositions were measured on powders, glass and magnetic fractions
26 387 (Electronic Appendix 1). The activity ratios ($^{230}\text{Th}/^{232}\text{Th}$) range between 0.262 in 0704-PN
27 388 powder and 0.654 in N-PON glass. These values are much lower than those reported for
28 389 historical lavas, which show small variations between 0.915 and 0.944 (Sigmarsson et al.,
29 390 2005; Pietruszka et al., 2009). Conversely, the ($^{230}\text{Th}/^{232}\text{Th}$) ratios of the pumice samples are
30 391 very similar to their ($^{238}\text{U}/^{232}\text{Th}$) ratios, which range between 0.240 and 0.689. This translates
31 392 into 0-14 % (average of 4.7%) excesses of ^{230}Th over ^{238}U (Fig. 6). However, errors of 6% on
32 393 ($^{238}\text{U}/^{232}\text{Th}$) ratios place five out of the six data points within error of equilibrium. Note that
33 394 all Th isotope data are relative to the zircon-free phase, because the digestion method used
34 395 may not fully dissolve zircons.
35
36
37
38
39
40
41
42
43
44

45 397 Oxygen isotopes

46 398
47
48
49 399 The two pumice powders analysed have $\delta^{18}\text{O}$ between +5.55 ‰ (sample 0704-PS) and +5.81
50 400 ‰ (sample 0704-PN) (Electronic Appendix 1). These values are within the range for mantle-
51 401 derived magmas, but are higher than the $\delta^{18}\text{O}$ of recent (1977-1992) steady state basalts,
52 402 which varies between +5.34 and +5.52 ‰ with an average of +5.40 ‰ (Boivin & Bachèlery,
53 403 2009). They are closer to the $\delta^{18}\text{O}$ range of Piton de la Fournaise 1977-1992 olivine rich lavas
54 404 (+5.52 to +5.72 ‰, average of +5.60 ‰; Boivin & Bachèlery, 2009).
55
56
57
58
59
60

406 **Lithium isotopes**

407
408 Vlastelic et al. (2011) previously noted that the low Li contents of samples 0704-PS and 0704-
409 PN (1 and 1.4 ppm, respectively) correlates with extremely low $\delta^7\text{Li}$ (-21 and -17‰,
410 respectively). By comparison, bulk analysis of different chips from the new sample 0704-TRA
411 yields even lower Li contents (between 0.48 and 0.13 ppm), but more variable and higher $\delta^7\text{Li}$
412 (between -7.2 and +13.8 ‰, Electronic Appendix 1). In situ Li isotope and major element
413 measurements were performed in sample 0704-TRA to constrain the origin of Li isotope
414 heterogeneity (Fig. 7). $\delta^7\text{Li}$ varies between -19.8 and -31.0 ‰ in the trachyte glass, and
415 between -3.1 and -30.7 ‰ in the glassy regions with abundant sub-micrometric K-feldspars
416 (Electronic Appendix 3). The interior of the trachyte pumice (7-9 mm from the basalt coating)
417 is more depleted in Li than the external 1 mm layer, due to a larger amount of feldspar
418 microlites in the glass and/or Li degassing. In situ analysis of the basaltic glass coating 0704-
419 TRA yields $\delta^7\text{Li}$ between +7.5 and +18.4 ‰, which is significantly heavier than bulk glass
420 composition (+4.2 ‰). Reporting all data in a $\delta^7\text{Li}$ vs. Li concentration plot (Fig. 8) highlights
421 two main arrays: SIMS data acquired on the pure trachytic glass show a positive correlation
422 between $\delta^7\text{Li}$ and Li content, while most other data acquired on sample regions with variable
423 microlite contents show the opposite relationship. The two arrays intercept at Li= 2 ppm and
424 $\delta^7\text{Li} = -35$ ‰. Two SIMS analyses (b9 and b22) performed close to the pumice surface (Fig. 7)
425 plot between this common component and the basalt composition (Fig. 8).

426 427 **DISCUSSION**

428 429 **Isotope constraints on the origin of the trachyte melt**

430
431 The isotope compositions of Sr, Nd and Pb indicate that the April 2007 trachyte shares the
432 same source as La Réunion basalts (Fig. 5), and is not produced by partial melting of the
433 underlying Indian Ocean crust, or another genetically unrelated lithology. For the same
434 reason, partial melting of an enriched mantle lithology, as proposed for other Mauritian
435 trachytes (Ashwal et al., 2016), or contamination from assimilated sediments (Sigmarsson et
436 al., 2013), can also be ruled out. The mantle-like $\delta^{18}\text{O}$ signature of the trachyte (+5.55 to +5.81

1
2
3 437 ‰) also precludes significant interaction with isotopically light (-8.67 to -4.9 ‰) hydrothermal
4
5 438 fluids (Bénard et al., 2020). The basalt coating the pumice has a relatively unradiogenic Pb
6
7 439 signature ($^{206}\text{Pb}/^{204}\text{Pb}$ of 18.873, Fig. 5b) that characterizes the lavas emitted on April 5 2007,
8
9 440 all other lavas from this eruption have $^{206}\text{Pb}/^{204}\text{Pb}$ between 18.902 and 18.911 (Vlastelic et al.,
10
11 441 2009b). The unradiogenic Pb isotope ratio indicates that the trachyte was emitted during the
12
13 442 eruption paroxysm on April 5 when the lava effusion rate transiently exceeded 200 m³/s, the
14
15 443 highest value ever measured at Piton de la Fournaise (Coppola et al., 2009). The mobilization
16
17 444 and eruption of the trachyte is thus clearly related to the unusual dynamics and/or path of
18
19 445 April 2007 magmas.

20 446 Previous studies (Falco, 2009; Salaün et al. 2010) noted that the Piton de la Fournaise 2007
21
22 447 trachyte plots at the end of the main differentiation trend of La Réunion basalts, showing a
23
24 448 similar composition as Piton des Neiges trachytes (Fig. 3). Salaün et al. (2010) suggested that
25
26 449 the major element composition of the trachyte is attainable through basalt crystallization,
27
28 450 although they acknowledged that the low-pressure (<800 MPa) line of descent that fits basalt
29
30 451 compositions does not reproduce more evolved compositions. Generally, available data
31
32 452 supports the idea that the 2007 trachyte is a differentiation product of La Réunion common
33
34 453 basalts. However, the extensive depletion (>90 %) of a number of volatile and semi-volatile
35
36 454 elements (F, Cl, B, Cs, Cu, Li), and the significant depletion of less volatile U (26-68%) are
37
38 455 testament to a complex history of storage and outgassing discussed here below.

38 456

39 457 **Lithium isotope constraints on volatile element loss**

40 458

41
42 459 Lithium has proved useful to reconstruct magma degassing owing to its affinity for aqueous
43
44 460 fluids and high diffusivity in silicate melts (Berlo et al., 2004; Kuritani & Nakamura, 2006; Kent
45
46 461 et al., 2007; Rowe et al., 2008; Koga et al., 2008; Vlastelic et al., 2013a). Lithium isotopes also
47
48 462 provide additional constraints on degassing processes (Beck et al., 2004; Schiavi et al., 2009;
49
50 463 Vlastelic et al., 2011): at equilibrium conditions, preferential partitioning of ⁷Li into aqueous
51
52 464 fluids (e.g., Wunder et al., 2006) decreases the ⁷Li/⁶Li ratio in the residual melt. Conversely,
53
54 465 out of equilibrium, faster diffusion of ⁶Li (Richter et al., 2003; Holycross et al., 2018) towards
55
56 466 the silicate melt-fluid interface increases ⁷Li/⁶Li of the melt. To a first order, the bulk Li
57
58 467 depletion and low ⁷Li/⁶Li of the pumice are consistent with equilibrium loss of Li. In detail, the
59
60 468 in situ SIMS data show two main orthogonal arrays in the $\delta^7\text{Li}$ versus Li plot that depart from

1
2
3 469 an end-member composition (Li=2ppm and $\delta^7\text{Li} = -35 \text{ ‰}$) (Fig. 8). The array with a positive
4
5 470 slope defined by the pure trachyte glass is thought to have preserved the equilibrium
6
7 471 distribution of Li isotopes acquired prior to sample disruption. The array with a negative slope
8
9 472 defined by the glass hosting sub-micrometric K-feldspars is consistent with disequilibrium loss
10
11 473 of Li during the exhumation of the trachyte melt by the April 2007 magma. This second event
12
13 474 of Li degassing might reflect slightly slower cooling of the interior of the pumice, which
14
15 475 allowed crystal nucleation and Li diffusion towards the gas-melt interface. In support of this
16
17 476 idea, Li is estimated to diffuse from melt to gas bubbles over time scales as short as seconds
18
19 477 (see last figure of Vlastelic et al., 2013a). In the following, we model the array of the pure glass
20
21 478 in order to constrain the degassing history of the trachyte melt prior to its exhumation. We
22
23 479 use the term "degassing" *sensu lato* for the exsolution of gas or fluid, in the absence of
24
25 480 constraints on the density of the exsolved phase.

25 481 We consider four scenarios, in which crystallization and degassing occurred simultaneously or
26
27 482 successively, in open or closed system. For simultaneous crystallization and degassing in an
28
29 483 open system we use the model previously developed for chlorine (Villemant & Boudon, 1999;
30
31 484 Villemant et al., 2008) and subsequently modified by Vlastelic et al. (2011) to account for Li
32
33 485 partitioning into minerals. During this fractional process referred to as FCD, fluids and crystals
34
35 486 are extracted from the silicate melt immediately after their formation. The concentration of
36
37 487 Li in the residual silicate melt (C^M) varies with the initial melt content (C_0^M) as follows (Eq. 1):

$$38 \quad 488$$

$$39 \quad 489 \quad C^M = C_0^M \cdot F^{(\beta - 1)}$$

$$40 \quad 490$$

41
42
43 491 *with*

$$44 \quad 492 \quad F = 1 - (1 + k)\Delta\text{Fluid}$$

45
46
47 493 *and*

$$48 \quad 494 \quad \beta = \frac{D^{V-M} + kD^{S-M}}{k + 1}$$

$$49 \quad 495$$

50
51
52
53
54 496 where F is the mass fraction of residual silicate melt, ΔFluid is the mass fraction of fluid lost,
55
56 497 and k the mass ratio of precipitated crystals to exsolved fluid. The latter (k) is assumed
57
58 498 constant although this parameter might increase during degassing–crystallization evolution
59
60

(Villemant et al., 2008). D^{V-M} and D^{S-M} are the fluid-melt and crystal-melt partition coefficients, respectively. Writing Eq.1 for each Li isotope, and normalising yields (Eq. 2) :

$$\left(\frac{{}^7\text{Li}}{{}^6\text{Li}}\right)^M = \left(\frac{{}^7\text{Li}}{{}^6\text{Li}}\right)_0^M \cdot F^{(\beta_7 - \beta_6)}$$

where $({}^7\text{Li}/{}^6\text{Li})_0^M$ is the initial isotopic ratio of the melt, and subscripts 7 and 6 denote for ${}^7\text{Li}$ and ${}^6\text{Li}$ species, respectively. In the second scenario referred to as ECD, crystallization and degassing occur simultaneously in closed-system, with melt, crystals and fluids remaining in chemical equilibrium. The expression of Li concentration in the silicate melt is obtained by combining the mass balance equation and the definition of β (Eq.3):

$$C^M = \frac{C_0^M}{\beta + F(1 - \beta)}$$

And for Li isotopes (Eq. 4):

$$\left(\frac{{}^7\text{Li}}{{}^6\text{Li}}\right)^M = \left(\frac{{}^7\text{Li}}{{}^6\text{Li}}\right)_0^M \frac{\beta_6 + F(1 - \beta_6)}{\beta_7 + F(1 - \beta_7)}$$

In Eq. 2 and 4, D_7^{V-M} and D_6^{V-M} are related through the coefficient of isotopic fractionation between fluid and silicate melt (α^{V-M}) defined as (Eq. 5):

$$\alpha^{V-M} = \frac{\left(\frac{{}^7\text{Li}}{{}^6\text{Li}}\right)^V}{\left(\frac{{}^7\text{Li}}{{}^6\text{Li}}\right)^M} = \frac{D_7^{V-M}}{D_6^{V-M}}$$

where $({}^7\text{Li}/{}^6\text{Li})^V$ is the Li isotopic composition of the fluid.

For both FCD and ECD, the primary melt is assumed to have 5.5 ppm Li (average content of melt inclusions hosted in olivine crystals with forsterite contents in the range of 83.4-83.9 %, Di Muro et al., 2014). Because Li isotopes do not fractionate significantly during crystallization

1
2
3 525 (Tomascak et al., 1999; Schuessler et al., 2009), we assume that the initial Li isotopic
4 526 composition is as in SSB ($\delta^7\text{Li}=+3.5\text{‰}$), and $D_7^{S-M} = D_6^{S-M}$ in Eq. 2 and 4. We then consider a
5 527 two-step process where degassing occurs after fractional crystallization (FC). The Li content of
6 528 the trachyte melt prior to degassing is estimated assuming no anomaly on trace element
7 529 patterns ($\text{Li}=\text{Li}_{\text{SSB}} \cdot [\text{Tm}/\text{Tm}_{\text{SSB}} + \text{Yb}/\text{Yb}_{\text{SSB}}]/2=11.8\text{ ppm}$), which implies a solid-melt partition
8 530 coefficient of ca. 0.6. Subsequent degassing is modelled using Eqs. (1-2) for fractional
9 531 degassing (open system) and Eqs. (3-4) for equilibrium degassing (closed-system) setting in
10 532 both cases $k=0$ (no crystallization). These two two-step processes are referred to as FC-FD and
11 533 FC-ED, respectively.

12 534 For all four scenarios, we consider a dominantly aqueous fluid, with a concentration of 1.0
13 535 wt.% in primary melts (Bureau et al., 1999; Di Muro et al., 2014). The H_2O content of the
14 536 trachyte melt prior to degassing (FC-FD and FC-ED processes) is estimated at 5.0 wt.%
15 537 assuming 80% crystallization of an anhydrous mineral assemblage (Upton & Wadsworth,
16 538 1972). Taking 0.2 wt.% for the final water content in the degassed trachyte (Vlastelic et al.,
17 539 2011), the amount of water lost (ΔFluid) is 0.8 wt.% in the FCD and ECD scenarios (with
18 540 $k=80/0.8$) and 4.8 wt.% in the FC-FD and FC-ED scenarios. With these parameters, the target
19 541 composition of the devolatilized trachyte ($\text{Li}=2\text{ ppm}$ and $\delta^7\text{Li} = -35\text{‰}$) requires D^{V-M} between
20 542 37 and 260 and α^{V-M} between 1.022 and 1.053 depending on the crystallization-degassing
21 543 scenario (Fig. 8). Only the FC-ED scenario with $D^{V-M}=104$ and $\alpha^{V-M}=1.048$ reproduces the linear
22 544 array shown by the trachyte glass data (Fig. 8). This indicates that the exsolved fluid remained
23 545 in equilibrium with the silicate melts, and suggests that the trachyte melt degassed in closed-
24 546 system. The idea that the fluid phase was not extracted until the disruption of the trachyte
25 547 melt by the basaltic magma is independently supported by the abnormally heavy $^7\text{Li}/\text{Li}^6$ (+7 to
26 548 +14‰) and slight positive Li anomaly of the basaltic glass coating the pumice (Fig. 4 and 8).
27 549 This signature is best explained if the 2007 basalt assimilated or interacted with the ^7Li -
28 550 enriched vapour derived from the trachyte melt. The fluid in equilibrium with the trachyte
29 551 glass (3.2-5.6 ppm Li and $\delta^7\text{Li}$ between -19.8 and -31‰) must have 331-583 ppm Li and $\delta^7\text{Li}$
30 552 between +16.1 and +26.1‰ (with $D^{V-M}=104$ and $\alpha^{V-M}=1.048$), and can thus easily contaminate
31 553 the basalt. If differentiation took place in the lithospheric mantle (at 30 km depth), which
32 554 cannot be ruled out, the parental melt would contain $1.1 \pm 0.9\text{ wt.}\%$ CO_2 in addition to 1.0

1
2
3 555 wt.% H₂O (Boudoire et al., 2018), and D^{V-M} would be 17-67 % lower than estimated above (but
4
5 556 α^{V-M} would not change markedly).
6
7 557

8
9 558 **Constraints on the density of the fluid phase from element partitioning between fluid and**
10 **silicate melt**
11 559

12 560
13
14 561 Lithium isotope variations imply that the trachyte parental melt did not reach water saturation
15
16 562 until the very late stage of crystallization. On the other hand, it is likely that the silicate melt
17
18 563 reached sulphide saturation in response to the drop of oxygen fugacity related to
19
20 564 titanomagnetite removal at MgO~5 wt.% (Collins et al., 2012). Lithium isotope evidence for
21
22 565 equilibrium degassing (FC-ED process) provides the possibility to estimate fluid-melt partition
23
24 566 coefficients for semi-volatile elements other than Li. The assumption behind this calculation
25
26 567 is that semi-volatile elements behave similar to lithium and concentrate in the trachyte melt
27
28 568 before being degassed. Concentrations of Cl, F, B, Cu and U in the trachyte melt prior to
29
30 569 degassing are estimated assuming that the element ratios Cl/Nb, F/Nd, B/Nb, Cs/Th, Cu/Th
31
32 570 and U/Th do not largely fractionate during crystallization, and are thus as in SSB (Electronic
33
34 571 Appendix 1). Fluid-melt partition coefficients are inferred from Eq. (3) with $\beta=D^{V-M}$ ($k=0$) and
35
36 572 $\Delta\text{Fluid} = 4.8$ wt.% (cf. previous section). In the absence of in situ glass data for the elements
37
38 573 of interest, we use the bulk concentration of 0704-PS and 0704-PN. We find D^{V-M} in the range
39
40 574 of $7.1-17 \times 10^2$ for Cs, $8.2-14 \times 10^2$ for Cu, $2.4-4.1 \times 10^2$ for F, $2.4-3.6 \times 10^2$ for Cl, 2.4×10^2 for
41
42 575 B and 8-47 for U. Note that these simple estimates are bulk partition coefficients of elements
43
44 576 between the trachytic melt and a fluid which composition is not constrained. The
45
46 577 corresponding concentrations of elements in the fluid in equilibrium with the trachyte melt
47
48 578 are 2.8 wt.% Cl, 2.4 wt.% F, 1.2 wt.% Cu, 480 ppm B, 30 ppm Cs and 20-46 ppm U. Although
49
50 579 the calculated D^{V-M} have a factor of two uncertainty, they are much larger than those
51
52 580 estimated at low pressure between silicate melt and low-density vapours, which are generally
53
54 581 close to unity or lower (Pokrovski et al., 2013). For instance, the partition coefficients of Li, Cs,
55
56 582 and Cu between gas and magma are estimated to be lower than 0.1 at Tolbachik, Kudryavy
57
58 583 and Erta Ale volcanoes (Zelenski et al., 2014). Conversely, the estimated D^{V-M} are comparable
59
60 584 to the partition coefficients measured between dense brines and silicate melts at crustal
585
586 585 conditions (600-1000 °C, 50-500 MPa) (Williams-Jones & Heinrich, 2005; Pokrovski et al.,
2013). The estimated mobility of uranium is even higher than in crustal fluids (Peiffert et al.,

1
2
3 587 1996), and approaches U behaviour in subduction zones fluids (Bali et al., 2011). Such elevated
4
5 588 partition coefficients reflect the complexation of metals and metalloids by halogen ions and
6
7 589 hydration, which increase with fluid salinity, density and pressure. This effect is especially
8
9 590 marked in the case investigated here as closed system degassing of the trachyte contributed
10
11 591 to maintain high concentrations of water, Cl and F in the system. The high D^{V-M} estimated for
12
13 592 Cu might also reflect to some extent the partitioning of Cu into liquid sulphides. Generally,
14
15 593 these results indicate that the trachyte parental magma most likely differentiated deeper than
16
17 594 the shallow magma reservoir of Piton de la Fournaise located at a depth of ca. 2.5 km.

18 595 19 20 596 **Uranium loss**

21 597
22
23 598 The depletion of U relative to Th in the pumice, with Th/U up to 12.7 against 4.0 in parental
24
25 599 basalts, indicates up to 68 % U removal. Fractional crystallisation of zircon, in which U strongly
26
27 600 partitions relative to Th, can be shown to have barely increased the Th/U in the 2007 trachyte.
28
29 601 Zircon is present in such a small abundance and sizes that it was not identified microscopically,
30
31 602 only different chemical dissolution techniques revealed its presence in the pumice. To
32
33 603 evaluate the fraction of zircon removed from the melt, we use the composition of the zircon-
34
35 604 free glass (sample dissolution in PTFE vials using HF-HNO₃) because the bulk rock contains
36
37 605 accumulative zircon as evidenced by Zr-Hf positive anomalies in trace element patterns (Fig.
38
39 606 4). The zircon-free glass shows up to 50% Zr depletion (Zr/Zr* of 0.5 in chip#1 of sample 0704-
40
41 607 TRA, which has 199 ppm Zr; Electronic Appendix 1). That glass thus misses up to 200 ppm Zr,
42
43 608 which corresponds to only 0.04% modal zircon (because the element zirconium (Zr)
44
45 609 corresponds to approximately half the weight of a zircon). How much zircon fractionated from
46
47 610 the trachyte melt can then be estimated for 80% fractional crystallisation of basalt (Upton &
48
49 611 Wadsworth, 1972) by multiplying the modal proportion of zircon with that of the remaining
50
51 612 melt proportion, namely $0.04\% \times 20\%$, or $8 \times 10^{-3} \%$. Assuming that U and Th do not
52
53 613 significantly enter major minerals, and zircon-melt partition coefficients of 81 for U and 8.2
54
55 614 for Th (Wang et al. 2011), 80% crystallization of a mineralogical assemblage including 8×10^{-3}
56
57 615 % zircon increases the Th/U ratio by a factor of 1.01 only. Thus, the amount of zircon removed
58
59 616 is too small to produce significant Th/U variations.

60 617 A more likely possibility is related to the increasing mobility of uranium in oxidising conditions.
618 618 Pietruszka et al. (2009) suggested that some lavas of Piton de la Fournaise assimilated plutonic

1
2
3 619 rocks enriched in U through the circulation of hydrothermal fluids. In their model,
4
5 620 hydrothermal fluids leach U^{6+} in the shallow oxidized layers of the volcanic edifice and
6
7 621 precipitate U^{4+} in the deeper more reduced regions. In the case of the U depleted rhyolite
8
9 622 pumice produced in 2011 at El Hierro (Canary islands), Sigmarsson et al. (2013) suggested that
10
11 623 assimilation of sediments raised the oxygen fugacity of the mingled rhyolitic magmas to near
12
13 624 Ni-NiO buffer, which enabled U volatilization as UF_6 . As discussed above, neither radiogenic
14
15 625 nor O isotopes provide evidence for assimilation of foreign material in the case studied here.
16
17 626 Moreover, lack of U enrichment in Piton de la Fournaise gas sublimates, including sulphates
18
19 627 and fluorides formed above thick lava flows (Vlastelic et al., 2013b), indicates that U is not
20
21 628 significantly transported by low pressure - low density vapours. In keeping with Li isotope
22
23 629 systematics, it is suggested that closed-system devolatilization of the trachyte melt during the
24
25 630 very late stage of differentiation produced fluids enriched chlorine, fluorine and possibly
26
27 631 carbonate (Upton & Wadsworth, 1972), leading to high solubility of U relative to Th. Whether
28
29 632 the fluid exsolved and remained as an immiscible phase together with the degassed trachytic
30
31 633 melt, or if it was integrated into hydrous phases (e.g., amphibole, chlorite, biotite ..)
32
33 634 crystallising from the fluid phase remains an open question.

34 635 35 636 **Age of U loss**

36 637
37
38 638 Constraints on the age of the U loss may be obtained from U-series decay products. Trachyte
39
40 639 melt formed by 80% fractional crystallisation from a basalt should have identical U/Th as the
41
42 640 parental magma, if the zircon proportion in the crystallising assemblage is very small. The very
43
44 641 low U/Th is thus compatible with U-loss by volatile exsolution from the trachyte melt (Fig. 6a).
45
46 642 Whether the volatile exsolution occurred instantaneously or progressively cannot be resolved
47
48 643 by the present results. Nevertheless, the radioactive equilibrium between ^{238}U and ^{230}Th (Fig.
49
50 644 6a) indicates that the minimum time elapsed since U loss is close to five times the half-life of
51
52 645 ^{230}Th , i.e. $5 \times 75.4 = 380$ ka, the time needed for reaching radioactive equilibrium between ^{238}U
53
54 646 and ^{230}Th . The small ^{230}Th excess measured in the glass fraction of sample 0704-TRA possibly
55
56 647 results from the contamination of the trachyte glass with small amount of 2007 basalt with
57
58 648 excess ^{230}Th over ^{238}U , which was the carrier magma for the old trachyte. This is consistent
59
60 649 with the observation that the basaltic glass locally invades the pumice as fine droplets or thin
60 650 films (Fig. 2a and c). However, such a contamination cannot explain the large variations of

1
2
3 651 ($^{230}\text{Th}/^{232}\text{Th}$) and ($^{238}\text{U}/^{232}\text{Th}$) in the trachyte samples, which most likely reflect mixing with the
4
5 652 U enriched fluids that did not escape. Indeed, the fluid composition is expected to plot on the
6
7 653 equiline on the other side of the equipoint (Fig. 6b), and may mix to some degree with the
8
9 654 trachyte melt if the system remained closed until the eruption.

10 655 The fractionation between U and Th is recorded at the end of ^{238}U and ^{232}Th decay chains by
11 656 ^{206}Pb and ^{208}Pb . The ten trachyte samples analysed for Pb isotopes show subtle variations of
12 657 the radiogenic $^{208}\text{Pb}^*/^{206}\text{Pb}^*$ ratio (0.9895-0.9918) within the range of historical basalts (Fig.
13 658 9). The $^{208}\text{Pb}^*/^{206}\text{Pb}^* - ^{232}\text{Th}/^{238}\text{U}$ isochron has a low and poorly defined slope of $1.7(\pm 8.3) \cdot 10^{-5}$,
14 659 which translates into an age of $0.37 \pm_{-0.37}^{+1.73}$ Ma. This imprecise age has little significance, but its
15 660 upper limit within error constrains Th/U fractionation to be younger than 2.1 Ma. In any case,
16 661 if the Th/U increase was older than 2.1 Ma, $^{208}\text{Pb}^*/^{206}\text{Pb}^*$ of the trachyte would be significantly
17 662 higher than the SSB value of 0.991 ± 0.002 (Vlastelic et al., 2006). Taken together, U-series
18 663 isotopes and $^{208}\text{Pb}^*/^{206}\text{Pb}^*$ constrain U loss to have occurred between 0.38 and 2.1 Ma ago.
19 664 Placing these ages in the history of La Réunion Island, we note that they span a time period
20 665 extending from the oldest subaerial activity of Piton des Neiges to the early activity of Piton
21 666 de la Fournaise (Fig. 10).

22 667

23 668 **Long-term trachyte storage**

24 669

25 670 The surprisingly old age of U loss raises the possibility, not envisioned so far, that the trachyte
26 671 derives from the remelting of ancient intrusive rocks of La Réunion Island. This possibility is
27 672 consistent with the basalt/trachyte volume ratio of about 10^8 , and the high temperature (1188
28 673 ± 16 °C, Gurioli et al., 2018) and fast ascent of 2007 magmas, which potentially allowed
29 674 important superheating above the liquidus. However, partial melting of gabbros with Zr deficit
30 675 (Zr/Zr^* in the range of 0.37-0.53, Nauret et al., 2019) cannot produce the 2007 trachyte with
31 676 a Zr excess (Zr/Zr^* of 1.6-3.0). Similarly, partial melting of plagioclase-free wehrlite cannot
32 677 produce the observed negative Sr-Ba-Eu anomalies (Fig. 4). In contrast, partial defrosting, or
33 678 melting of a solidified syenite intrusion is compatible with the 2007 trachyte composition.
34 679 Depletion of Sr, Ba and Eu (Fig. 4) and low K/Zr would suggest feldspar-rich residue rather than
35 680 alkali feldspar cumulate melting in the “trachyte attractor” hypothesis of Wolff (2017). Indeed,
36 681 the major element concentrations of the 2007 trachyte are within the range of glasses formed
37 682 by partial melts of syenite from Ascension Island (Harris & Bell, 1982), with the noticeable

1
2
3 683 exception of Na₂O. Unfortunately, trace element concentrations have not been determined
4
5 684 on those glasses to the best of our knowledge. The exsolved fluid phase would then have been
6
7 685 stored in the ubiquitous hydrous phases (amphibole, chlorite and/or biotite) or interstitial
8
9 686 cavities, such as those described by Upton & Wadsworth (1972) in microsyenites from Piton
10
11 687 des Neiges.

12 688 In a second scenario, slow crystallization could have lasted at least approximately 0.4 Ma and
13
14 689 a trachytic melt could still be available within the magma plumbing system, either as
15
16 690 interstitial melt in a crystal mush or as melt lens. To survive over such time scale, a small
17
18 691 volume of silicic magma requires a perfect balance of heat flux, so that melts neither solidify
19
20 692 nor float and escape. To evaluate this possibility, we estimate the volume of Piton de la
21
22 693 Fournaise plumbing system which temperature is maintained above the trachyte liquidus
23
24 694 (about 800°C) due to the continuous flux of hot basaltic magma. The thermal power Q brought
25
26 695 by the incoming magma depends on the magma flux (ϕ), the temperature difference between
27
28 696 magma reservoir (T_{res}) and injected magma (T_{inj}), and the fraction of crystal removed (f) at T_{res}
29 697 according to (Eq. 6):

$$Q = \phi \rho (C_p (T_{inj} - T_{res}) + fL)$$

30
31 698
32
33 699
34 700
35
36 701 where ρ is the magma density (2600 kg/m³), C_p the heat capacity (1500 J/kg per K) and L the
37
38 702 latent heat (4x10⁵ J/kg) (Hawkesworth et al., 2000). Independent observations, including the
39
40 703 age/volume ratio of La Réunion edifice (e.g. de Voogd et al., 1999) and the small Sr isotope
41
42 704 variations of lavas (Vlastelic et al., 2018), suggest that the long-term magma production rate
43
44 705 has remained relatively uniform and similar to the average rate over the last 60 years (0.5
45
46 706 m³/s, dense rock equivalent, Roult et al., 2012). Based on the MELTS modeling of Villemant et
47
48 707 al. (2009), we set $T_{inj} = 1304^\circ\text{C}$ and $T_{res} = 1150^\circ\text{C}$ with $f=0.2$ for Steady State Basalt with 92 ppm
49
50 708 Ni (Electronic Appendix 1). Using these values, Q is estimated at 4×10^8 W. We assume that
51
52 709 this thermal power is uniformly emitted in a spherical plumbing system with a steady-state
53
54 710 thermal structure. The temperature decreases from the centre to the boundary of the sphere
55
56 711 according to Eq. 4.42 of Turcotte & Schubert (1982) (Eq. 7):

$$T_x = T_{x=r} + \frac{\rho H}{6k} (r^2 - x^2)$$

714
 715 where $r(m)$ is the radius of the sphere, $x(m)$ the distance to its centre, H the heat supply in W
 716 per kg, and k the thermal conductivity ($2.24 W/m$ per K). Substituting $Q(W)$ for $H(W/kg)$, the
 717 sphere radius writes (Eq. 8):

$$r = \frac{Q}{8k\pi(T_c - T_{x=r})}$$

720
 721 where T_c is the temperature at the centre of the sphere. Using a temperature of $1150^\circ C$ at the
 722 center of the plumbing system (i.e., $T_c = T_{res}$) and $200^\circ C$ at its boundary (2.5-4 km depth at 50-
 723 $80^\circ C/km$, Dezayes et al., 2016), the sphere radius is estimated at 7.5 km. Note that this value
 724 is robust because Q is rather well constrained and the temperature difference between the
 725 center and the boundary of the plumbing system must be close to $1000^\circ C$. From Eq.7 the
 726 sphere with $T > 800^\circ C$ has a radius of 4.6 km and its volume represents about $\frac{1}{4}$ of the
 727 plumbing system. This hot core could correspond to the central plumbing system of Piton de
 728 la Fournaise located below the enclos Fouqué caldera (Fig. 1; Michon et al., 2015). This simple
 729 model indicates that the thermal flux from hot basaltic magmas raising from the mantle is high
 730 enough to prevent magmas trapped within the central plumbing system of Piton de la
 731 Fournaise from total solidification. Whether the old trachyte erupted in 2007 is related to the
 732 fading sub-terrain magmatic activity of older volcanoes on La Réunion, Piton des Neiges or Les
 733 Alizés, is not clear but its origin could be contemporaneous with the initiation of Piton de la
 734 Fournaise volcano (Fig. 10).

735 736 **CONCLUSIONS**

737
 738 This paper aims to understand the eruption of a small volume of silicic melt during the largest
 739 historical eruption of the Piton de la Fournaise volcano. Such an event is puzzling because the
 740 volcano has regularly produced very homogeneous basalts since 0.44 Ma. The in-depth
 741 geochemical study of the pumice samples confirms previous suggestions that the trachyte is
 742 a differentiation product of a common basalt. On the other hand, the trachyte shows two
 743 particular geochemical features that may be testament to a long and complex history of
 744 differentiation and outgassing: (1) the extensive depletion of moderately volatile elements

1
2
3 745 (Cs, B, Li, Cu) and uranium, together with large Li isotope fractionation are consistent with
4
5 746 closed system exsolution of dense fluids at a depth of several kilometres. (2) U-series isotopes
6
7 747 and radiogenic $^{208}\text{Pb}^*/^{206}\text{Pb}^*$ constrain the time elapsed since U loss to between 0.4 and 2.1
8
9 748 Ma. Because this age is as old or older than Piton de la Fournaise shield edifice, the 2007
10
11 749 trachyte could be a product of an ancient volcano, such as Piton des Neiges or Les Alizés, which
12
13 750 declined about 0.4 Ma ago. Alternatively, it could result from the remobilization of the
14
15 751 interstitial melt of a micro-syenite intrusion, possibly not fully solidify due to the sustained
16
17 752 heat supply from hot basaltic magmas. The unusual dynamics of April 2007 eruption certainly
18
19 753 played a major role in remobilizing the old trachyte, providing the first direct evidence for
20
21 754 silicic melts in the plumbing system of Piton de la Fournaise basaltic volcano.
22

23 755

24 756 **Funding**

25 757 This research was financed by the French Government Laboratory of Excellence initiative n°
26
27 758 ANR-10-LABX-0006, the Region Auvergne and the European Regional Development Fund. This
28
29 759 is Laboratory of Excellence ClerVolc contribution number 484.
30

31 760

32 761 **Acknowledgements**

34 762 D. Auclair, M. Benbakkar, C. Bosq, G. Falco, C. Fonquernie, J.L. Piro (LMV Clermont-Ferrand),
35
36 763 P. Télouk (ENS Lyon), E. Deloule and the Ion Probe group from CRPG Nancy contributed to
37
38 764 data acquisition. We thank Nina Søger, Guillaume Girard and Marco Brenna for their
39
40 765 constructive comments, and Tod Waight for his useful remarks and for handling the
41
42 766 manuscript.
43

44 767

1
2
3 768 Figure captions
4

5 769

6
7 770 Figure 1

8
9 771 Location maps. (a) Shaded relief map of La Réunion Island showing major structural features,
10 772 modified from Gailler and Lénat (2012). The boundary between Piton des Neiges (PdN) and
11 773 Piton de la Fournaise (PdF) volcanoes, and the locations of the main places discussed in the
12 774 text are shown. The main vent of the April 2007 eruption (Piton Tremblet shown with a star)
13 775 is located within the Enclos Fouqué caldera, along the SE rift zone. Older calderas of Piton de
14 776 la Fournaise are labelled. Note that the Rivière des Remparts caldera hosts the major outcrop
15 777 of 400-530 ka old differentiated lavas, recently ascribed to the vanishing activity of an older
16 778 volcano (named Les Alizés), which was active in the SE of the island prior to Piton de la
17 779 Fournaise (Valer et al., 2017a). Seismic zones labelled [N30–40] and [N120] (dashed lines) are
18 780 interpreted as representing magma path 40-30 and 20-11 km below sea level, respectively,
19 781 below the western flank of Piton de la Fournaise (Michon et al. 2015, 2016; Boudoire et al.,
20 782 2017). Following the April 2007 eruption, several earthquakes clustered 30km below sea level,
21 783 30 km to the west of Piton de la Fournaise summit [2007DEC], suggesting that the April 2007
22 784 magmas rose through a very eccentric region of the deep plumbing system. (b) Map of the
23 785 April 2007 eruptive vent showing the opening fracture (dashed line), the Piton Tremblet (dark
24 786 grey), the lava flow (light grey), and the pumice fallout (hatched field). The pumices were
25 787 grouped according to their location relative to the opening fracture: the PN field
26 788 ($21^{\circ}16'53.5\pm 4.5''S - 55^{\circ}46'19\pm 4''E$) is located to the SW of the fracture whereas the PS field
27 789 ($21^{\circ}16'50\pm 2''S - 55^{\circ}46'27\pm 4''E$) is located to the NE. Few chips from each fields were
28 790 powdered for bulk chemical analyses (0704-PN and 0704-PS samples). White pumices with
29 791 trace of basaltic glass were found to the North of Piton Tremblet at the border of the April
30 792 2007 lava flow ($21^{\circ}16'51''S - 55^{\circ}46'29''E$). They are referred to as sample 0704-TRA. Chips
31 793 from the PN (N-PON) and PS (S-PON and 0704-TRA) fields were selected for in situ analysis.
32 794 (a&b) Coordinates are in km (WGS84, UTM 40S). (c) Photo of the pumice and its basaltic glass
33 795 coating (N-PON sample).

34 796

35
36 797 Figure 2

37
38 798 Images of the pumice samples. (a) Close-up view of the relationship between basaltic (dark)
39 799 and trachytic (white) glasses (N-PON sample). 1- Mixing zone with characteristic round

1
2
3 800 vesicles. 2- Fine droplets of basaltic liquid impregnating the trachytic pumice. (b) Scanning
4
5 801 Electron Microscope (SEM) image of pumice 0704-PS showing a highly vesiculated texture
6
7 802 with thin glassy vesicle walls. (c) Transmitted plane-polarized photomicrograph of SPON3
8
9 803 sample with brown glass coating trachytic glass; (d) Backscatter Scanning Electron Microscope
10
11 804 (BSE) image of the same field as (c) Mgt = magnetite crystals. Plg = microlites of plagioclase.
12
13 805 (e) BSE image of the transition from basaltic to trachytic liquids illustrating the gradual change
14
15 806 in composition and crystallization of plagioclase (Plg) microcrystals in the basaltic glass
16
17 807 (sample SPON3). (f) BSE image showing the development of abundant alkali feldspar (Fth)
18
19 808 micro-crystallization in trachytic glass (sample SPON1). Note the presence of a cluster of
20
21 809 magnetite crystals in the trachytic liquid close to its contact with a more basic liquid. In all
22
23 810 panels, the yellow numbers express the SiO₂ content (wt.%).

23 811
24
25 812 **Figure 3**
26
27 813 Total alkali vs. silica (TAS) diagram (Le Bas et al., 1986) showing representative compositions
28
29 814 of the trachytic pumices. Bulk rock compositions (circles) are from this study and Falco (2009).
30
31 815 The compositional fields of Piton des Neiges and Piton de la Fournaise volcanoes are reported.

32 816
33
34 817 **Figure 4**
35
36 818 Trace element patterns of the April 2007 trachytic pumice and the basaltic coating.
37
38 819 Concentrations are normalized to the average concentrations of steady-state basalts (SSB)
39
40 820 given in Electronic Appendix 1. SSB are the dominant homogeneous basalts of La Réunion
41
42 821 Island (Albarède et al., 1997). Pattern of 0704-PS is drawn using the data obtained with
43
44 822 NH₄HF₂ dissolution. Pattern of 0704-PS is drawn combining data obtained with Savillex (Li, Cs,
45
46 823 Pb) and alkali fusion (other elements) dissolution methods. Pattern of 0704-TRA is the mean
47
48 824 of analyses of chips #1-4 (Savillex) with Zr-Hf data from chip#7 analysis (Parr 250°C). Vertical
49
50 825 lines indicate elements with negative anomalies.

51 826
52
53 827 **Figure 5**
54
55 828 Sr-Nd-Pb isotope plots. The signature of the trachytic pumice and the basaltic coating is
56
57 829 compared to that of La Réunion lavas in ¹⁴³Nd/¹⁴⁴Nd vs ⁸⁷Sr/⁸⁶Sr (a) and ²⁰⁸Pb/²⁰⁴Pb vs
58
59 830 ²⁰⁶Pb/²⁰⁴Pb (b) spaces. The ¹⁴³Nd/¹⁴⁴Nd ratios are shown using the εNd notation where
60
831 $\epsilon\text{Nd} = [({}^{143}\text{Nd}/{}^{144}\text{Nd})_{\text{sample}} / ({}^{143}\text{Nd}/{}^{144}\text{Nd})_{\text{CHUR}} - 1] \cdot 10^4$ with $({}^{143}\text{Nd}/{}^{144}\text{Nd})_{\text{CHUR}} = 0.512638$. Error

bars are shown in (a) and are within data symbols in (b). Data used to draw the La Réunion isotopic fields are from Fisk et al. (1988), Fretzdorff & Haase (2002), Bosch et al. (2008), Pietruszka et al. (2009), Smietana (2011), Vlastelic et al. (2005, 2007, 2009b, 2018).

Figure 6

($^{230}\text{Th}/^{232}\text{Th}$) versus ($^{238}\text{U}/^{232}\text{Th}$) isochron plot. (a) The composition of historical lavas of Piton de la Fournaise (black field) is drawn using the data of Sigmarsson et al. (2005) and Pietruszka et al. (2009). Errors bars of ($^{230}\text{Th}/^{232}\text{Th}$) and ($^{238}\text{U}/^{232}\text{Th}$) are either shown or within symbol size. All but one trachyte samples plot within error on the equiline, which is indicative of ^{230}Th - ^{238}U radioactive equilibrium. Indicative isochrons are shown for different values of t, using the equation:

$$\left(\frac{^{230}\text{Th}}{^{232}\text{Th}}\right) = \left(\frac{^{230}\text{Th}}{^{232}\text{Th}}\right)^0 e^{-\lambda^{230}.t} + \left(\frac{^{238}\text{U}}{^{232}\text{Th}}\right)(1 - e^{-\lambda^{230}.t})$$

where t is the age of Th/U fractionation and λ^{230} is the decay constants for ^{230}Th . Dashed lines show 20% and 40% ^{230}Th -excesses, i.e. ($^{230}\text{Th}/^{238}\text{U}$) = 1.2 and 1.4, respectively. (b) Schematic illustration of how the 2007 trachyte formed. Fractional crystallisation yields trachyte melt with identical ($^{230}\text{Th}/^{232}\text{Th}$) and ($^{238}\text{U}/^{232}\text{Th}$) as the parental basalt (assumed to be identical to the recent basalts). During final magma differentiation (t=0), exsolution of fluids in which U partitions, but not Th, yields U-poor trachyte melt (horizontal arrows) and important ^{238}U - ^{230}Th disequilibria. Both the ^{238}U -depleted trachyte and the ^{238}U -enriched fluid age and strive towards ^{238}U - ^{230}Th equilibrium (broken vertical arrows). Radioactive equilibrium is established after approximately 0.4 Ma with the U-depleted trachyte and the U-rich fluid having acquired a very low and very high ($^{230}\text{Th}/^{232}\text{Th}$), respectively. At any time, the residual melt and the fluid plot on an isochron, on each side of the equipoint. If the system remained closed, mixing between melt and fluid could explain the large variation of melt composition along the equiline (Fig. 6 a). If the melt and the volatiles have remained as liquid and fluid phases since over 0.4 Ma, a special thermal regime is requested beneath Piton de la Fournaise. Alternatively, the trachyte crystallised as micro-syenite and the volatile phase as hydrous minerals both of which were defrosted by the primitive 2007 basalt. Both these possibilities are discussed in the text.

1
2
3 863
4

5 864 **Figure 7**

6
7 865 Schematic cross section of sample 0704-TRA showing the loci of in situ Li isotope analyses. (a)
8 866 Most analyses were done in the basalt coating (grey) and nearby in the trachyte (white). Ol:
9 867 olivine crystals. (b) Three analyses were done in the interior of the pumice, 7-9 mm from the
10 868 basalt coating. (c) Example of a SEM image acquired after SIMS measurements. These images
11 869 were used to distinguish analyses performed on pure trachytic glass (light colour) from those
12 870 done on glassy regions with abundant sub-micrometric K-feldspars (dark colour).
13
14
15
16
17

18 871

19
20 872 **Figure 8**

21 873 $\delta^7\text{Li}$ versus Li concentration plot. Degassing and crystallization of a primary melt with 5.5 ppm
22 874 Li and $\delta^7\text{Li}=+3.5\text{‰}$ (star labelled PM) is modelled considering four scenarios: Fractional
23 875 Crystallization (FC) followed by Fractional Degassing (FD) or Equilibrium degassing (ED);
24 876 simultaneous crystallization and degassing in an open system (FCD) or closed system (ECD).
25 877 Depending on the crystallization-degassing scenario, the target composition of the
26 878 devolatilized trachyte (Li=2 ppm and $\delta^7\text{Li} = -35\text{‰}$) requires D^{V-M} between 37 and 260 and α^{V-M}
27 879 between 1.022 and 1.053. Only the FC-ED scenario with $D^{V-M}=104$ and $\alpha^{V-M}=1.048$
28 880 reproduces the linear array shown by the trachyte glass data (white diamonds). See text for
29 881 detailed description of the model and related equations and assumptions. The field of Piton
30 882 de la Fournaise (dark grey) is drawn using the data of Vlastelic et al. (2011).
31
32
33
34
35
36
37
38
39

40 883

41
42 884 **Figure 9**

43 885 $^{208}\text{Pb}^*/^{206}\text{Pb}^*$ versus $^{232}\text{Th}/^{238}\text{U}$ isochron plot. $^{208}\text{Pb}^*/^{206}\text{Pb}^* = \frac{[(^{208}\text{Pb}/^{204}\text{Pb})_S - (^{208}\text{Pb}/^{204}\text{Pb})_{\text{CD}}]}{[(^{206}\text{Pb}/^{204}\text{Pb})_S - (^{206}\text{Pb}/^{204}\text{Pb})_{\text{CD}}]}$ where subscripts S and CD refer to sample and
44 886 Canyon Diablo meteorite, respectively. $(^{208}\text{Pb}/^{204}\text{Pb})_{\text{CD}}=29.476$ and $(^{206}\text{Pb}/^{204}\text{Pb})_{\text{CD}}=9.307$
45 887 (Tatsumoto et al., 1973). The slope-age relationship in this isochron diagram is given by:
46 888
47
48
49
50

51 889

$$^{208}\text{Pb}^* / ^{206}\text{Pb}^* = \frac{\kappa_1 \mu_1 (e^{(\lambda^{232}.T)} - e^{(\lambda^{232}.t)}) + \kappa_2 \mu_2 (e^{(\lambda^{232}.t)} - 1)}{\mu_1 (e^{(\lambda^{238}.T)} - e^{(\lambda^{238}.t)}) + \mu_2 (e^{(\lambda^{238}.t)} - 1)}$$

52
53
54 890

55
56
57 891
58
59
60

1
2
3 892 where $T=4.56$ Ga, t is the age of Th/U fractionation, and λ^{232} and λ^{238} are the decay constants
4
5 893 for ^{232}Th and ^{238}U . κ and μ are the $^{232}\text{Th}/^{238}\text{U}$ and $^{238}\text{U}/^{204}\text{Pb}$ atomic ratios, respectively.
6
7 894 Subscripts 1 and 2 are relative to the intervals 4.56 Ga - t and t - 0 Ga, respectively. Indicative
8
9 895 isochrons are shown for t in the range of 5 Ma – 4.56 Ga (plain lines). The regression line
10
11 896 through trachyte data (dashed line) constrains Th/U fractionation to be younger than 2.1 Ma.
12
13 897

14 898 Figure 10

15
16 899 Temporal compositional evolution of La Réunion Island volcanoes. The $\text{CaO}/\text{Al}_2\text{O}_3$ ratio is used
17
18 900 as a proxy for magma differentiation. Regression line through Piton des Neiges differentiated
19
20 901 series (white triangles) is shown, whereas only temporal trends are shown for Piton des Neiges
21
22 902 and Piton de la Fournaise shield stages because major elements and ages were not measured
23
24 903 on same samples. The age estimated for the parental basalt of the 2007 trachyte is indicated
25
26 904 (hatched area). The 2007 trachyte plots on the temporal compositional trend of the Piton des
27
28 905 Neiges differentiated series, suggesting it could be a liquid remnant of the extinct volcano.
29
30 906 Data source: McDougall (1971), Oversby (1972), Upton & Wadsworth (1972), Gillot & Nativel
31
32 907 (1982), Albarède et al. (1997), Valer et al. (2017a).
33
34
35
36
37
38
39
40
41
42
43
44
45
46
47
48
49
50
51
52
53
54
55
56
57
58
59
60

References

- Albarède, F. (1993) Residence time analysis of geochemical fluctuations in volcanic series. *Geochimica et Cosmochimica Acta* **57**, 615-621.
- Albarède, F., Luais, B., Fitton, G., Semet, M., Kaminski, E., Upton, B.G.J., Bachèlery, P. & Cheminée, J.L. (1997) The geochemical regimes of Piton de la Fournaise volcano (Réunion) during the last 530 000 years. *Journal of Petrology* **38**, 171-201.
- Ashwal, L., Torsvik, T., Horvath, P., Harris, C., Webb, S., Werner, S. & Corfu, F. (2016) A Mantle-derived Origin for Mauritian Trachytes. *Journal of Petrology* **57**, 1645–1675.
- Bachèlery, P., Saint-Ange, F., Villeneuve, N., Savoye, B., Normand, A., Le Drezen, E., Barrère, A., Quod, J.-P. & Deplus, C. (2010). Huge lava flows into the sea and caldera collapse, April 2007, Piton de la Fournaise volcano. IAVCEI Third Workshop on Collapse Calderas, La Réunion, 3-9 October 2010, 73-74.
- Bali, E., Audétat, A. & Keppler, H. (2011) The mobility of U and Th in subduction zone fluids: an indicator of oxygen fugacity and fluid salinity. *Contributions to Mineralogy and Petrology* **161**, 597–613.
- Beck, P., Barrat, J.A., Chaussidon, M., Gillet, P. & Bohn, M. (2004) Li isotopic variations in single pyroxenes from the Northwest Africa 480 shergottite (NWA 480): a record of degassing of Martian magmas ? *Geochimica et Cosmochimica Acta* **68**, 2925-2933.
- Bénard, B., Famin, V., Agrinier, P., Aunay, B., Lebeau, G., Sanjuan, B., Vimeux, F., Bardoux, G. & Dezayes, C. (2020) Origin and fate of hydrothermal fluids at Piton des Neiges volcano (Réunion Island): A geochemical and isotopic (O, H, C, Sr, Li, Cl) study of thermal springs. *Journal of Volcanology and Geothermal Research* **392**, 106682.
- Berlo, K., Blundy, J., Turner, S., Cashman, K., Hawkesworth, C. & Black, S. (2004) Geochemical precursors to volcanic activity at Mount St. Helens, USA. *Science* **306**, 1167-1169.
- Bindeman, I., Gurenko, A., Sigmarsson, O., & Chaussidon, M. (2008). Oxygen isotope heterogeneity and disequilibria of olivine crystals in large volume Holocene basalts from Iceland: Evidence for magmatic digestion and erosion of Pleistocene hyaloclastites. *Geochimica et Cosmochimica Acta* **72**, 4397–4420.
- Boivin, P. & Bachèlery, P. (2009) Petrology of 1977 to 1998 eruptions of Piton de la Fournaise, La Réunion Island. *Journal of Volcanology and Geothermal Research* **184**, 109-105.

- 1
2
3 939 Bosch, D., Blichert-Toft, J., Moynier, F., Nelson, B.K., Télouk, P., Gillot, P.-Y. & Albarède, F.
4
5 940 (2008) Pb, Hf and Nd isotope compositions of the two Réunion volcanoes (Indian Ocean):
6
7 941 A tale of two small-scale mantle "blobs"? *Earth and Planetary Science Letters* **265**, 748-
8
9 942 768.
- 10 943 Boudoire, G., Liuzzo, M., Di Muro, A., Ferrazzini, V., Michon, L., Grassa, F., Derrien, A.,
11 944 Villeneuve, N., Bourdeu, A., Brunet, C., Giudice, G. & Gurrieri, S. (2017) Investigating the
12 945 deepest part of a volcano plumbing system: evidence for an active magma path below
13 946 the western flank of Piton de la Fournaise (La Réunion Island). *Journal of Volcanology*
14 947 *and Geothermal Research* **341**, 193–207.
- 15 948 Boudoire, G., Rizzo, A.L., Di Muro, A., Grassa, F. & Liuzzo M. (2018) Extensive CO₂ degassing
16 949 in the upper mantle beneath oceanic basaltic volcanoes: First insights from Piton de la
17 950 Fournaise volcano (La Réunion Island). *Geochimica et Cosmochimica Acta* **235**, 376–401.
- 18 951 Bureau, H., Métrich, N., Semet, M. & Staudacher, T. (1999) Fluid-magma decoupling in a hot-
19 952 spot volcano. *Geophysical Research Letters* **23**, 3501-3504.
- 20 953 Carpentier, M., Gannoun, A., Pin, C. & Sigmarsson, O. (2015) New Thorium Isotope Ratio
21 954 Measurements in Silicate Reference Materials: A-THO, AGV-2, BCR-2, BE-N, BHVO-2 and
22 955 BIR-1. *Geostandards and Geoanalytical Research*, doi: 10.1111/j.1751-
23 956 908X.2015.00385.x.
- 24 957 Collins, S.J., Maclennan, J., Pyle, D.M., Barnes, S.J. & Upton, B.G.J. (2012) Two phases of
25 958 sulphide saturation in Réunion magma: Evidence from cumulates. *Earth and Planetary*
26 959 *Science Letters* **337-338**, 104-113.
- 27 960 Coppola, D., Piscopo, D., Staudacher, T. & Cigolini, C. (2009) Lava discharge rate and effusive
28 961 pattern at Piton de la Fournaise from MODIS data. *Journal of Volcanology and*
29 962 *Geothermal Research* **184**, 174-192.
- 30 963 Coppola, D., Di Muro, A., Peltier, A., Villeneuve, N., Ferrazzini, V., Favalli, M., Bachèlery, P.,
31 964 Gurioli, L., Harris, A.J.L., Moune, S., Vlastélic, I., Galle, B., Arellano, S. & Aiuppa, A. (2017)
32 965 Shallow system rejuvenation and magma discharge trends at Piton de la Fournaise
33 966 volcano (La Réunion Island). *Earth and Planetary Science Letters* **463**, 13–24.
- 34 967 Chauvel, C., Bureau, S. & Poggi, C. (2011) Comprehensive chemical and isotopic analyses of
35 968 basalt and sediment reference materials. *Geostandards and Geoanalytical Research* **35**,
36 969 125-143.
37
38
39
40
41
42
43
44
45
46
47
48
49
50
51
52
53
54
55
56
57
58
59
60

- 1
2
3 970 Deniel, C., Kieffer, G. & Lecointre, J. (1992) New ^{230}Th - ^{238}U and ^{14}C age determinations from
4
5 971 Piton des Neiges volcano, Reunion — A revised chronology for the Differentiated Series.
6
7 972 *Journal of Volcanology and Geothermal Research* **51**, 253–267.
- 8
9 973 Deniel, C. & Pin, C. (2001) Single-stage method for the simultaneous isolation of lead and
10
11 974 strontium from silicate samples for isotopic measurements. *Analytica Chimica Acta* **426**,
12
13 975 95–103.
- 14 976 Derrien, A. (2019) Apport des techniques photogrammétriques à l'étude du dynamisme des
15
16 977 structures volcaniques du Piton de la Fournaise. PhD thesis University Sorbonne Paris
17
18 978 Cité. 333 p.
- 19
20 979 de Voogd, B., Palomé, S.P., Hirn, A., Charvis, P., Gallart, J., Rousset, D., Danobeitia, J. &
21
22 980 Perroud, H. (1999) Vertical movements and material transport during hotspot activity:
23
24 981 Seismic reflection profiling offshore La Réunion. *Journal of Geophysical Research* **104**,
25
26 982 2855-2874.
- 27 983 Dezayes, C., Baltassat, J.M., Famin, V. & Bes de Berc, S., 2016. Potential interest areas for the
28
29 984 development of geothermal energy in La Reunion Island. European Geothermal
30
31 985 Congress, Sep 2016, Strasbourg, France.
- 32
33 986 Di Muro, A., Métrich, N., Vergani, D., Rosi, M., Armienti, P., Fougereux, T., Deloule, E.,
34
35 987 Arienzo, I. & Civetta, L. (2014) The shallow plumbing system of the Piton de la Fournaise
36
37 988 volcano (La Réunion Island, Indian Ocean) revealed by the major 2007 caldera-forming
38
39 989 eruption. *Journal of Petrology* **55**, 1287-1315.
- 40 990 Falco, G. (2009) Evolution magmatique au Piton de la Fournaise : Exemple de l'éruption
41
42 991 d'Avril 2007. Master 2 thesis, La Reunion University, 50 p.
- 43
44 992 Famin, V., Welsch, B., Okumura, S., Bachèlery, P., Nakashima, S. (2009) Three differentiation
45
46 993 stages of a single magma at Piton de la Fournaise volcano (Reunion hotspot).
47
48 994 *Geochemistry Geophysics Geosystems* **10**, Q01007, doi:10.1029/2008GC002015.
- 49 995 Fisk, M.R., Upton, B.G.J., Ford, C.E. & White, W.M. (1988). Geochemical and experimental
50
51 996 study of the genesis of magmas of Reunion Island, Indian Ocean. *Journal of Geophysical*
52
53 997 *Research* **93**, 4933-4950.
- 54
55 998 Fretzdorff, S. & Haase, K.M. (2002). Geochemistry and petrology of lavas from the submarine
56
57 999 flanks of Réunion Island (western Indian Ocean): implications for magma genesis and
58
59 1000 mantle source. *Mineralogy and Petrology* **75**, 153-184.
60

- 1
2
3 1001 Gailler L.-S. & Lénat J.-F. (2012) Internal architecture of La Réunion (Indian Ocean) inferred
4 from geophysical data. *Journal of Volcanology and Geothermal Research* **221–222**, 83–
5 1002 98.
6
7 1003
8
9 1004 Gansecki, C.A. & Lee, R.L. (2018) Andesite Erupted from Kilauea Volcano During the 2018
10 Eruption. American Geophysical Union, Fall Meeting, abstract V43J0260.
11 1005
12 1006 Gansecki, C.A., Lee, R.L., Shea, T., Lundblad, S.P., Hon, K. & Parcheta, C. (2019) The tangled
13 tale of Kīlauea’s 2018 eruption as told by geochemical monitoring. *Science* **366**,
14 1007 eaaz0147.
15 1008
16 1009
17 1010 Gillot, P.-Y. & Nativel, P. (1982) K-Ar chronology of the ultimate activity of Piton des Neiges
18 volcano, Reunion island, Indian Ocean. *Journal of Volcanology and Geothermal Research*
19 **13**, 131-146.
20 1011
21 1012 Gillot, P.-Y., Lefèvre, J.-C. & Nativel, P. (1994) Model for the structural evolution of the
22 volcanoes of Réunion Island. *Earth and Planetary Science Letters* **122**, 291-302.
23 1013
24 1014 Gurioli, L., Di Muro, A., Vlastélic, I., Moune, S., Villeneuve, N., Bachèlery, P., Valer, M., Thivet,
25 S., Boudoire, G., Peltier, A., Ferrazzini, V., Métrich, N., Benbakkar, M., Cluzel, N.,
26 Constantin, C., Devidal, J.-L., Fonquernie, C. & Hénot, J.-M. (2018) Integrating field,
27 1015 textural and geochemical monitoring to track eruption triggers and dynamics: a case-
28 study from Piton de la Fournaise. *Solid Earth* **9**, 431–455.
29 1016
30 1017
31 1018 Harris, C. & Bell, J.D. (1982) Natural Partial Melting of Syenite Blocks from Ascension Island.
32 *Contributions to Mineralogy and Petrology* **79**, 107-113.
33 1019
34 1020
35 1021 Hawkesworth, C.J., Blake, S., Evans, P., Hughes, R., MacDonald, R., Thomas, L.E., Turner, S.P.
36 & Zellmer, G. (2000) Time Scales of Crystal Fractionation in Magma Chambers -
37 Integrating Physical, Isotopic and Geochemical Perspective. *Journal of Petrology* **41**, 991-
38 1022 1006.
39 1023
40 1024
41 1025 Helz, R.T. (2008) How to Produce Dacitic Melt at Kilauea: Evidence from Historic Kilauea Lava
42 Lakes. American Geophysical Union, Fall Meeting, abstract V23A-2135.
43 1026
44 1027 Holycross, M.E., Watson, E.B., Richter, F.M. & Villeneuve, J. (2018) Diffusive fractionation of
45 Li isotopes in wet, highly silicic melts. *Geochemical Perspectives Letters* **6**, 39-42.
46 1028
47 1029 Kent, A.J.R., Blundy, J., Cashman, K.V., Cooper, K.M., Donnelly, C., Pallister, J.S., Reagan, M.,
48 Rowe, M.C. & Thornber, C.R. (2007) Vapor transfer prior to the October 2004 eruption
49 of Mount St. Helens, Washington. *Geology* **35**, 231-234.
50 1030
51 1031
52
53
54
55
56
57
58
59
60

1
2
3
4
5
6
7
8
9
10
11
12
13
14
15
16
17
18
19
20
21
22
23
24
25
26
27
28
29
30
31
32
33
34
35
36
37
38
39
40
41
42
43
44
45
46
47
48
49
50
51
52
53
54
55
56
57
58
59
60

- 1032 Koga, K.T., Cluzel, N., Rose-Koga, E.F., Laporte, D. & Shimizu, N. (2008), Experimental
1033 demonstration of lithium-boron depletion during magma degassing, *Eos Trans. AGU*,
1034 89(53), Fall Meet. Suppl., Abstract V31B-2143.
- 1035 Kuritani, T. & Nakamura, E. (2006) Elemental fractionation in lavas during post-eruptive
1036 degassing: Evidence from trachytic lavas, Rishiri Volcano, Japan. *Journal of Volcanology*
1037 *and Geothermal Research* **149**, 124-138.
- 1038 Le Bas, M.J., Le Maitre, R.W., Streckeisen, A. & Zanettin, B. (1986) A Chemical Classification
1039 of Volcanic Rocks Based on the Total Alkali-Silica Diagram. *Journal of Petrology* **27**, 745-
1040 750.
- 1041 Lénat, J.F., Bachèlery, P. & Merle, O. (2012) Anatomy of Piton de la Fournaise volcano (La
1042 Réunion, Indian Ocean). *Bulletin of Volcanology* **74**, 1945-1961.
- 1043 Macdonald, G. A. & Katsura, T. (1964) Chemical composition of Hawaiian lavas. *Journal of*
1044 *Petrology* **5**, 82–135.
- 1045 Martin, E. & Sigmarsson, O. (2007) Low-pressure differentiation of tholeiitic lavas as
1046 recorded in segregation veins from Reykjanes (Iceland), Lanzarote (Canary Islands) and
1047 Masaya (Nicaragua). *Contributions to Mineralogy and Petrology* **154**, 559-573.
- 1048 McDougall, I. (1971) The geochronology and evolution of the young volcanic island of
1049 Réunion, Indian Ocean. *Geochimica et Cosmochimica Acta* **35**, 261-288.
- 1050 Merle, O., Mairine, P., Michon, L., Bachèlery, P. & Smietana, M. (2010) Calderas, landslides
1051 and paleo-canyons on Piton de la Fournaise volcano (La Réunion Island, Indian Ocean).
1052 *Journal of Volcanology and Geothermal Research* **189**, 131–142.
- 1053 Michon, L., Ferrazzini, V., Villeneuve, N., Famin, V. & Di Muro, A. (2015) Rift zones and
1054 magma plumbing system of Piton de la Fournaise volcano: How do they differ from
1055 Hawaii and Etna? *Journal of Volcanology and Geothermal Research* **303**, 112–129.
- 1056 Michon, L., Ferrazzini, V. & Di Muro A (2016) Magma Paths at Piton de la Fournaise Volcano.
1057 In: Active Volcanoes of the Southwest Indian Ocean: Piton de la Fournaise and Karthala.
1058 Active Volcanoes of the World (eds Bachèlery, P., Lénat, J.-F., Di Muro, A., Michon, L.) P.
1059 91-206.
- 1060 Moore, J., White, W. M., Paul, D., Duncan, R. A., Abouchami, W. & Galer, S.G. (2011).
1061 Evolution of shield-building and rejuvenescent volcanism of Mauritius. *Journal of*
1062 *Volcanology and Geothermal Research* **207**, 47–66.

- 1
2
3 1063 Nauret, F., Famin, V., Vlastelic, I. & Gannoun, A. (2019) A trace of recycled continental crust
4
5 1064 in the Réunion hotspot. *Chemical Geology* **524**, 67-76.
6
7 1065 Oversby, V.M. (1972) Genetic relations among the volcanic rocks of Réunion: chemical and
8
9 1066 lead isotopic evidence. *Geochimica et Cosmochimica Acta* **36**, 1167-1179.
10
11 1067 Peiffert, C., Cuney, M. & Nguyen-Trung, C. (1996) Uranium in granitic magmas. Part 2:
12
13 1068 experimental determination of uranium solubility and fluid-melt partitioning
14
15 1069 coefficients in the uranium oxide-haplogranite-H₂O-NaX (X = Cl, F) system at 770°C 2
16
17 1070 kbar. *Geochimica et Cosmochimica Acta* **60**, 1515–1529.
18
19 1071 Peltier, A., Bachèlery, P. & Staudacher, T. (2009) Magma transport and storage at Piton de
20
21 1072 La Fournaise (La Réunion) between 1972 and 2007: a review of geophysical and
22
23 1073 geochemical data. *Journal of Volcanology and Geothermal Research* **184**, 93–108.
24
25 1074 Pietruszka, A.J., Hauri, E.H. & Blichert-Toft, J. (2009) Crustal contamination of mantle-derived
26
27 1075 magmas within Piton de la Fournaise Volcano, Réunion Island. *Journal of Petrology* **50**,
28
29 1076 661-684.
30
31 1077 Pin, C. & Zalduegui, J.F.S. (1997) Sequential separation of light rare-earth elements, thorium
32
33 1078 and uranium by miniaturized extraction chromatography: Application to isotopic
34
35 1079 analyses of silicate rocks. *Analytica Chimica Acta* **339**, 79-89.
36
37 1080 Pokrovski, G.S., Borisova, A.Y. & Bychkov A.Y. (2013) Speciation and Transport of Metals and
38
39 1081 Metalloids in Geological Vapors. *Reviews in Mineralogy & Geochemistry* **76**, 165-218.
40
41 1082 Richter, F.M., Davis, A.M., DePaolo, D.J. & Watson, E.B. (2003) Isotope fractionation by
42
43 1083 chemical diffusion between molten basalt and rhyolite. *Geochimica et Cosmochimica*
44
45 1084 *Acta* **67**, 3905-3923.
46
47 1085 Roult, G., Peltier, A., Staudacher, T., Ferrazzini, V., Taisne, B., Di Muro, A. & the OVPF team
48
49 1086 (2012) A new comprehensive classification of the Piton de la Fournaise activity spanning
50
51 1087 the 1985–2010 period. Search and analysis of short-term precursors from a broad-band
52
53 1088 seismological station. *Journal of Volcanology and Geothermal Research* **241-242**, 78-
54
55 1089 104.
56
57 1090 Rowe, M.C., Kent, A.J.R. & Thornber, C.R. (2008) Using amphibole phenocrysts to track vapor
58
59 1091 transfer during magma crystallization and transport: An example from Mount St. Helens,
60
1092 Washington. *Journal of Volcanology and Geothermal Research* **178**, 593-607.
1093
1094 Salaün, A., Villemant, B., Semet, M.P. & Staudacher, T. (2010) Cannibalism of olivine-rich
cumulate xenoliths during the 1998 eruption of Piton de la Fournaise (La Réunion

1
2
3
4
5
6
7
8
9
10
11
12
13
14
15
16
17
18
19
20
21
22
23
24
25
26
27
28
29
30
31
32
33
34
35
36
37
38
39
40
41
42
43
44
45
46
47
48
49
50
51
52
53
54
55
56
57
58
59
60

- hotspot): Implication for the generation of magma diversity. *Journal of Volcanology and Geothermal Research* **198**, 187-204.
- Schiavi, F., Kobayashi, K., Moriguti, T., Nakamura, E., Pompilio, M., Tiepolo, M., Vannuci, R. (2009). Degassing, crystallization and eruption dynamics at Stromboli: trace element and lithium isotopic evidence from 2003 ashes. *Contributions to Mineralogy and Petrology* **159**, 541–561.
- Schuessler, J.A., Schoenberg, R. & Sigmarsson, O. (2009) Iron and lithium isotope systematics of the Hekla volcano, Iceland — Evidence for Fe isotope fractionation during magma differentiation. *Chemical Geology* **258**, 78-91.
- Sigmarsson, O., Condomines, M. & Bachèlery, P. (2005) Magma residence time beneath the Piton de la Fournaise volcano, Réunion Island, from U-series disequilibria. *Earth and Planetary Science Letters* **234**, 223-234.
- Sigmarsson, O., Laporte, D., Carpentier, M., Devouard, B., Devidal, J.-L. & Marti, J. (2013) Formation of U-depleted rhyolite from a basanite at El Hierro, Canary Islands. *Contributions to Mineralogy and Petrology* **165**, 601–622.
- Smietana, M. (2011) Pétrologie, géochronologie (K-Ar) et géochimie élémentaire et isotopique (Sr, Nd, Hf, Pb) de laves anciennes de la Réunion: Implications sur la construction de l'édifice volcanique. PhD Thesis, Université de la Réunion, France.
- Staudacher, T., Ferrazzini, V., Peltier, A., Kowalski, P., Boissier, P., Catherine, P., Lauret, F. & Massin, F. (2009) The April 2007 eruption and the Dolomieu crater collapse, two major events at Piton de la Fournaise (La Réunion Island, Indian Ocean). *Journal of Volcanology and Geothermal Research* **184**, 126-137.
- Stieltjes, L. & Moutou, P. (1989) A statistical and probabilistic study of the historic activity of Piton de la Fournaise, Réunion Island, Indian Ocean. *Journal of Volcanology and Geothermal Research* **36**, 67-86.
- Tatsumoto, M., Knight, R.J. & Allègre, C.J. (1973) Time differences in the formation of meteorites as determined from the ratio of lead-207 to lead-206. *Science* **180**, 1279–1283.
- Teplov, W., Marsh, B., Hulen, J., Spielman, P., Kaleikini, M., Fitch, D. & Rickard, W. (2009) Dacite Melt at the Puna Geothermal Venture Wellfield, Big Island of Hawaii. *Geothermal Resources Council Transactions* **33**, 989-994.

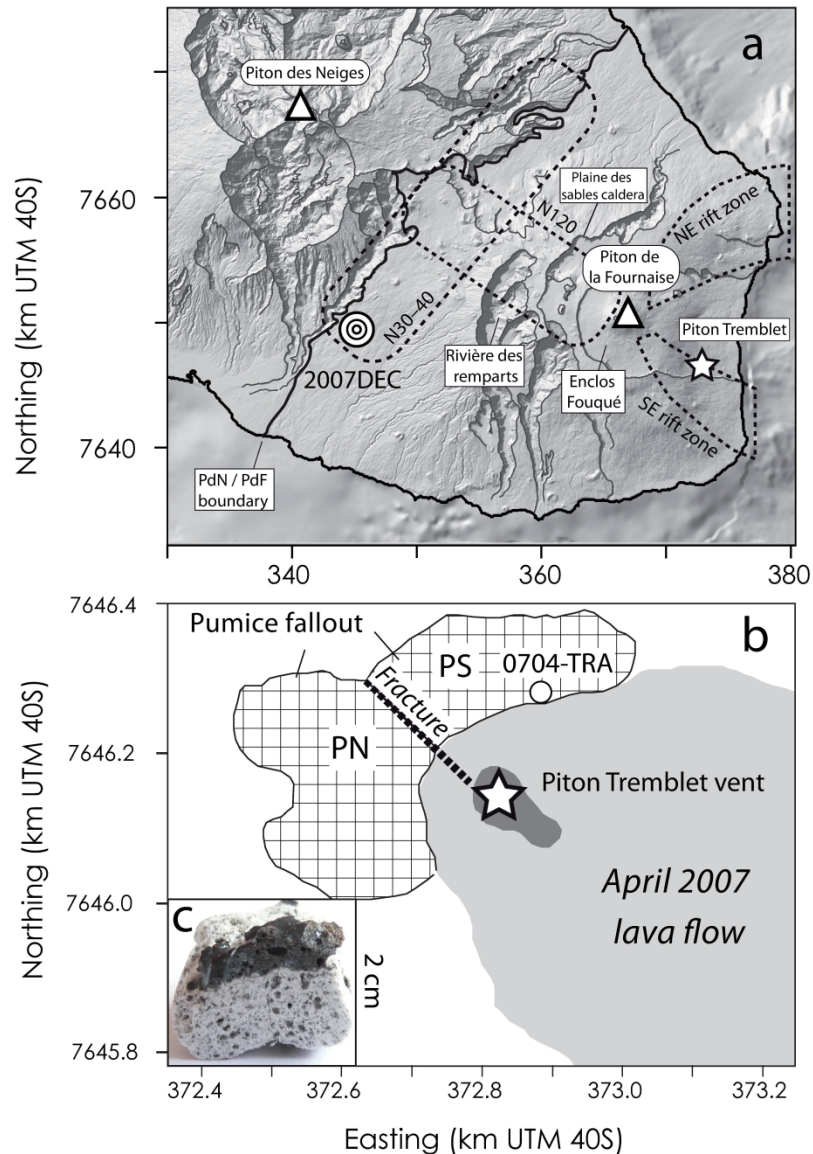
- 1
2
3 1126 Todt, W., Cliff, R.A., Hanser, A. & Hofmann, A.W. (1996) Evaluation of a ^{202}Pb - ^{205}Pb double
4
5 1127 spike for high-precision lead isotope analysis. In *Earth Processes: Reading the Isotopic*
6
7 1128 *Code*, AGU, A. Basu and S. Hart (Eds.), p 429-437.
- 8
9 1129 Tomascak, P.B., Tera, F., Helz, R.T. & Walker, R.J. (1999) The absence of lithium isotope
10
11 1130 fractionation during basalt differentiation: New measurements by multicollector ICP-
12
13 1131 MS. *Geochimica et Cosmochimica Acta* **63**, 907-910.
- 14 1132 Turcotte, D. & Schubert, G. *Geodynamics: Application of continuum physics to geological*
15
16 1133 *problems*, J. Wiley and Sons, New York, 1982, 450 pp.
- 17
18 1134 Upton, B.G.J. & Wadsworth, W.J. (1966) The basalts of Réunion Island, Indian Ocean. *Bulletin*
19
20 1135 *of Volcanology* **29**, 7-23.
- 21 1136 Upton, B.G.J. & Wadsworth, W.J. (1971) Rhyodacite glass in Réunion basalt. *Mineralogical*
22
23 1137 *Magazine* **38**, 152-159.
- 24
25 1138 Upton, B.G.J. & Wadsworth, W. J. (1972) Aspects of magmatic evolution on Réunion Island.
26
27 1139 *Philosophical Transactions of the Royal Society of London, Series A* **271**, 105–130.
- 28
29 1140 Valer, M., Bachèlery, P. & Schiano, P. (2017a) The Petrogenesis of Plagioclase-ultraphyric
30
31 1141 Basalts from La Réunion Island. *Journal of Petrology* **58**, 675–698.
- 32
33 1142 Valer, M., Bachèlery, P. & Schiano, P. (2017b) Geochemical characteristics of the La Réunion
34
35 1143 mantle plume source inferred from olivine-hosted melt inclusions from the adventive
36
37 1144 cones of Piton de la Fournaise volcano (La Réunion Island) *Contributions to Mineralogy*
38
39 1145 *and Petrology* **172**, 74.
- 40 1146 Valley, J.W., Kitchen, N.E., Kohn, M.J., Niendorf, C.R. & Spicuzza, M.J. (1995) UWG-2, a garnet
41
42 1147 standard for oxygen isotope ratio: Strategies for high precision and accuracy
43
44 1148 with laser heating. *Geochimica et Cosmochimica Acta* **59**, 5223–5231.
- 45 1149 Villemant, B. & Boudon, G. (1999) H₂O and halogen (F, Cl, Br) behaviour during shallow
46
47 1150 magma degassing processes. *Earth and Planetary Science Letters* **168**, 271-286.
- 48
49 1151 Villemant, B., Mouatt, J. & Michel, A. (2008) Andesitic magma degassing investigated
50
51 1152 through H₂O vapour-melt partitioning of halogens at Soufrière Hills Volcano,
52
53 1153 Montserrat (Lesser Antilles). *Earth and Planetary Science Letters* **269**, 212-229.
- 54 1154 Villeneuve, N. & Bachèlery, P. (2006) Revue de la typologie des éruptions au Piton de La
55
56 1155 Fournaise, processus et risques volcaniques associés. *Cybergeo: Eur J Geogr Environ Nat*
57
58 1156 *Paysage*, article 336. <http://cybergeo.revues.org/2536>. doi:10.4000/cybergeo.2536.
59
60

1
2
3
4
5
6
7
8
9
10
11
12
13
14
15
16
17
18
19
20
21
22
23
24
25
26
27
28
29
30
31
32
33
34
35
36
37
38
39
40
41
42
43
44
45
46
47
48
49
50
51
52
53
54
55
56
57
58
59
60

- Vlastélic, I., Staudacher, T. & Semet, M. (2005) Rapid change of lava composition from 1998 to 2002 at Piton de la Fournaise (Réunion) inferred from Pb isotopes and trace elements: evidence for variable crustal contamination. *Journal of Petrology* **46**, 79-107.
- Vlastélic, I., Lewin, E. & Staudacher, T. (2006) Th/U and other geochemical evidence for the Réunion plume sampling a less differentiated mantle domain. *Earth and Planetary Science Letters* **248**, 364-378.
- Vlastélic, I., Peltier, A. & Staudacher, T. (2007) Short-term (1998-2006) fluctuations of Pb isotopes at Piton de la Fournaise volcano (Réunion Island): Origins and constraints on the size and shape of the magma reservoir. *Chemical Geology* **244**, 202-220.
- Vlastélic, I., Koga, K., Chauvel, C., Jacques, G. & Télouk, P. (2009a) Survival of lithium isotopic heterogeneities in the mantle supported by HIMU-lavas from Rurutu Island, Austral Chain. *Earth and Planetary Science Letters* **286**, 456-466.
- Vlastélic, I., Deniel, C., Bosq, C., Télouk, P., Boivin, P., Bachèlery, P., Famin, V. & Staudacher, T. (2009b) Pb isotope geochemistry of Piton de la Fournaise historical lavas. *Journal of Volcanology and Geothermal Research* **184**, 63-78.
- Vlastélic, I., Staudacher, T., Bachèlery, P., Télouk, P., Neuville, D. & Benbakkar M. (2011) Lithium isotope fractionation during magma degassing: constraints from silicic differentiates and natural gas condensates from Piton de la Fournaise volcano (Réunion Island). *Chemical Geology* **284**, 26-34.
- Vlastélic, I., Menard, G., Gannoun A., Piro, J.-L., Staudacher, T. & Famin, V. (2013a) Magma degassing during the April 2007 collapse of Piton de la Fournaise: the record of semi-volatile trace elements (Li, B, Cu, In, Sn, Cd, Re, Tl, Bi). *Journal of Volcanology and Geothermal Research* **254**, 94-107.
- Vlastélic, I., Staudacher, T., Deniel, C., Devidal, J.L., Devouard, B., Finizola, A. & Télouk, P. (2013b) Lead isotopes behavior in the fumarolic environment of the Piton de la Fournaise volcano (Réunion Island). *Geochimica et Cosmochimica Acta* **100**, 297-314.
- Vlastélic, I. & Pietruszka, A.J. (2016) A review of the recent geochemical evolution of Piton de la Fournaise volcano, Réunion Island (1927-2010). In: *Active Volcanoes of the Southwest Indian Ocean: Piton de la Fournaise and Karthala. Active Volcanoes of the World* (eds Bachèlery, P., Lénat, J.-F., Di Muro, A., Michon, L.) p. 185-201.

- 1
2
3 1187 Vlastélic, I., Di Muro, A., Bachèlery, P., Gurioli, L., Gannoun, A. & Auclair, D. (2018) Control of
4
5 1188 source fertility on the eruptive activity of Piton de la Fournaise volcano, La Réunion.
6
7 1189 *Scientific Reports* **8**, Article number 14478.
- 8
9 1190 Wang, X., Griffin, W.L., Chen, J., Huang, P. & Li, X. (2011) U and Th Contents and Th/U Ratios
10
11 1191 of Zircon in Felsic and Mafic Magmatic Rocks: Improved Zircon-Melt Distribution
12
13 1192 Coefficients. *Acta Geologica Sinica* **85**, 164-174.
- 14 1193 Williams-Jones, A.E. & Heinrich, C.A. (2005) Vapor transport of metals and the formation of
15
16 1194 magmatic-hydrothermal ore deposits. *Economic Geology* **100**, 1287-1312.
- 17
18 1195 Wolff, J.A. (2017) On the syenite-trachyte problem. *Geology* **45**, 1067–1070.
- 19
20 1196 Wunder, B., Meixner, A., Romer, R.L. & Heinrich, W. (2006) Temperature-dependent isotopic
21
22 1197 fractionation of lithium between clinopyroxene and high-pressure hydrous fluids.
23
24 1198 *Contributions to Mineralogy and Petrology* **151**, 112–120.
- 25 1199 Zelenski M., Malik N. & Taran Y. (2014) Emissions of trace elements during the 2012–2013
26
27 1200 effusive eruption of Tolbachik volcano, Kamchatka: enrichment factors, partition
28
29 1201 coefficients and aerosol contribution. *Journal of Volcanology and Geothermal Research*
30
31 1202 **285**, 136-149.
- 32
33 1203 Zhang, W., Hu, Z., Liu, Y., Chen, H., Gao, S. & Gaschnig, R.M. (2012) Total Rock Dissolution
34
35 1204 Using Ammonium Bifluoride (NH₄HF₂) in Screw-Top Teflon Vials: A New Development in
36
37 1205 Open-Vessel Digestion. *Analytical chemistry* **84**, 10686–10693.
- 38
39
40
41
42
43
44
45
46
47
48
49
50
51
52
53
54
55
56
57
58
59
60

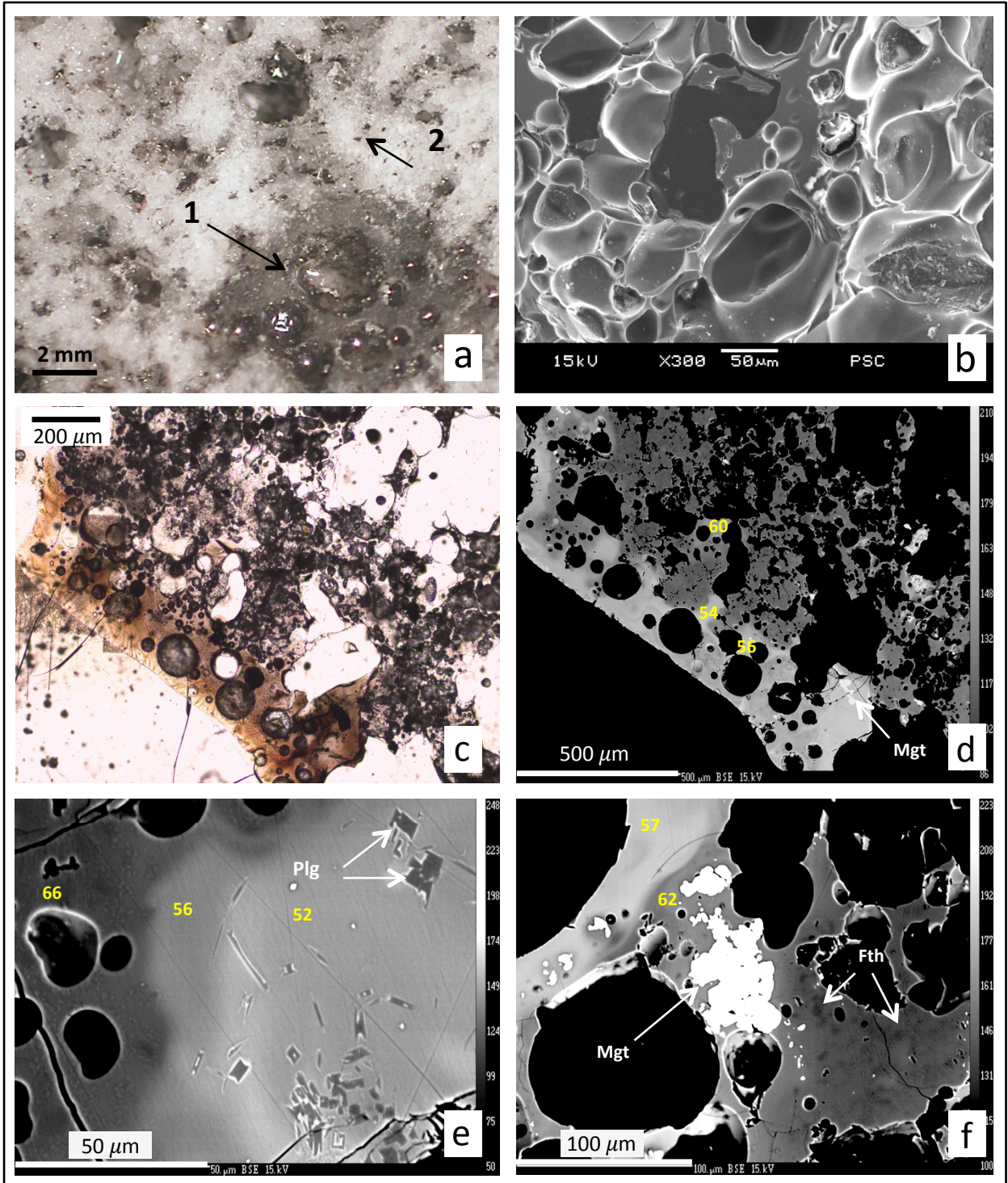
F1



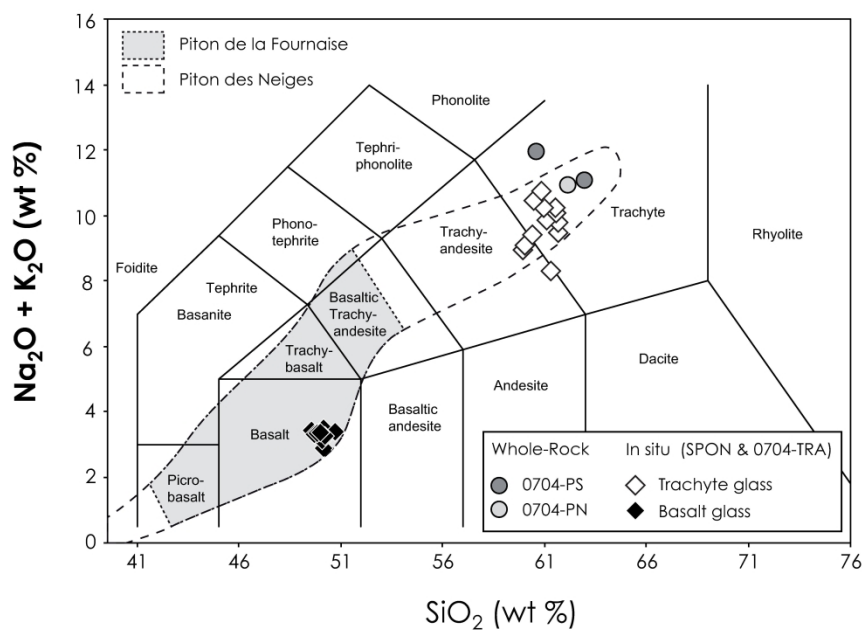
Location maps. (a) Shaded relief map of La Réunion Island showing major structural features, modified from Gailler and Lénat (2012). The boundary between Piton des Neiges (PdN) and Piton de la Fournaise (PdF) volcanoes, and the locations of the main places discussed in the text are shown. The main vent of the April 2007 eruption (Piton Tremblet shown with a star) is located within the Enclos Fouqué caldera, along the SE rift zone. Older calderas of Piton de la Fournaise are labelled. Note that the Rivière des Remparts caldera hosts the major outcrop of 400-530 ka old differentiated lavas, recently ascribed to the vanishing activity of an older volcano (named Les Alizés), which was active in the SE of the island prior to Piton de la Fournaise (Valer et al., 2017a). Seismic zones labelled [N30-40] and [N120] (dashed lines) are interpreted as representing magma path 40-30 and 20-11 km below sea level, respectively, below the western flank of Piton de la Fournaise (Michon et al. 2015, 2016; Boudoire et al., 2017). Following the April 2007 eruption, several earthquakes clustered 30km below sea level, 30 km to the west of Piton de la Fournaise summit [2007DEC], suggesting that the April 2007 magmas rose through a very eccentric region of the deep plumbing system. (b) Map of the April 2007 eruptive vent showing the opening fracture (dashed line), the Piton Tremblet (dark grey), the lava flow (light grey), and the pumice fallout (hatched field). The pumices

1
2
3 were grouped according to their location relative to the opening fracture: the PN field ($21^{\circ}16'53.5\pm 4.5''S -$
4 $55^{\circ}46'19\pm 4''E$) is located to the SW of the fracture whereas the PS field ($21^{\circ}16'50\pm 2''S - 55^{\circ}46'27\pm 4''E$) is
5 located to the NE. Few chips from each fields were powdered for bulk chemical analyses (0704-PN and
6 0704-PS samples). White pumices with trace of basaltic glass were found to the North of Piton Tremblet at
7 the border of the April 2007 lava flow ($21^{\circ}16'51''S - 55^{\circ}46'29''E$). They are referred to as sample 0704-
8 TRA. Chips from the PN (N-PON) and PS (S-PON and 0704-TRA) fields were selected for in situ analysis.
9 (a&b) Coordinates are in km (WGS84, UTM 40S). (c) Photo of the pumice and its basaltic glass coating (N-
PON sample).

10
11 190x271mm (600 x 600 DPI)
12
13
14
15
16
17
18
19
20
21
22
23
24
25
26
27
28
29
30
31
32
33
34
35
36
37
38
39
40
41
42
43
44
45
46
47
48
49
50
51
52
53
54
55
56
57
58
59
60



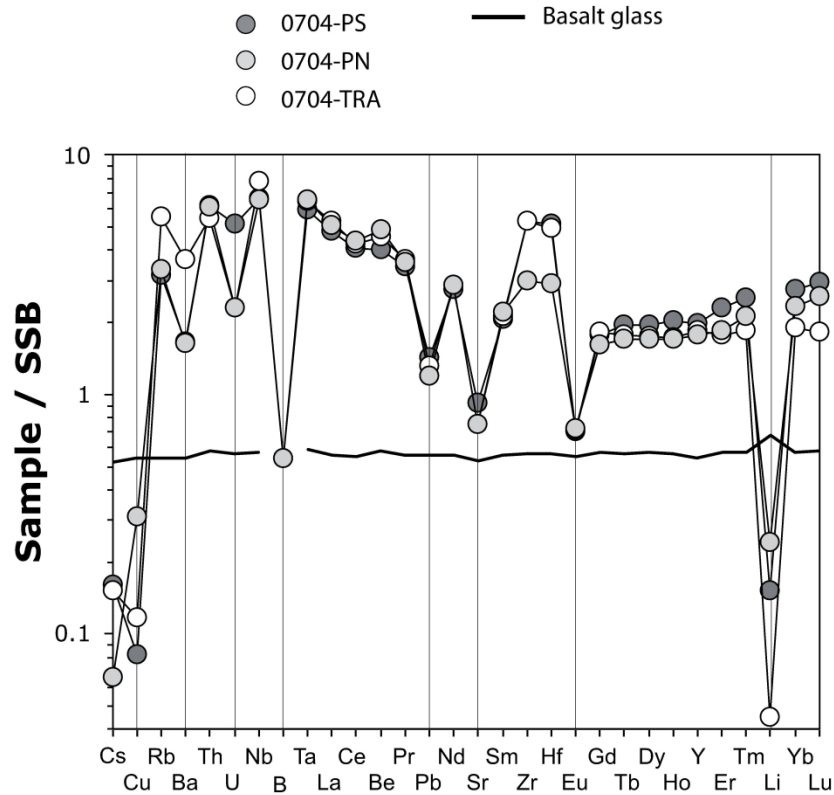
F3



Total alkali vs. silica (TAS) diagram (Le Bas et al., 1986) showing representative compositions of the trachytic pumices. Bulk rock compositions (circles) are from this study and Falco (2009). The compositional fields of Piton des Neiges and Piton de la Fournaise volcanoes are reported.

251x239mm (600 x 600 DPI)

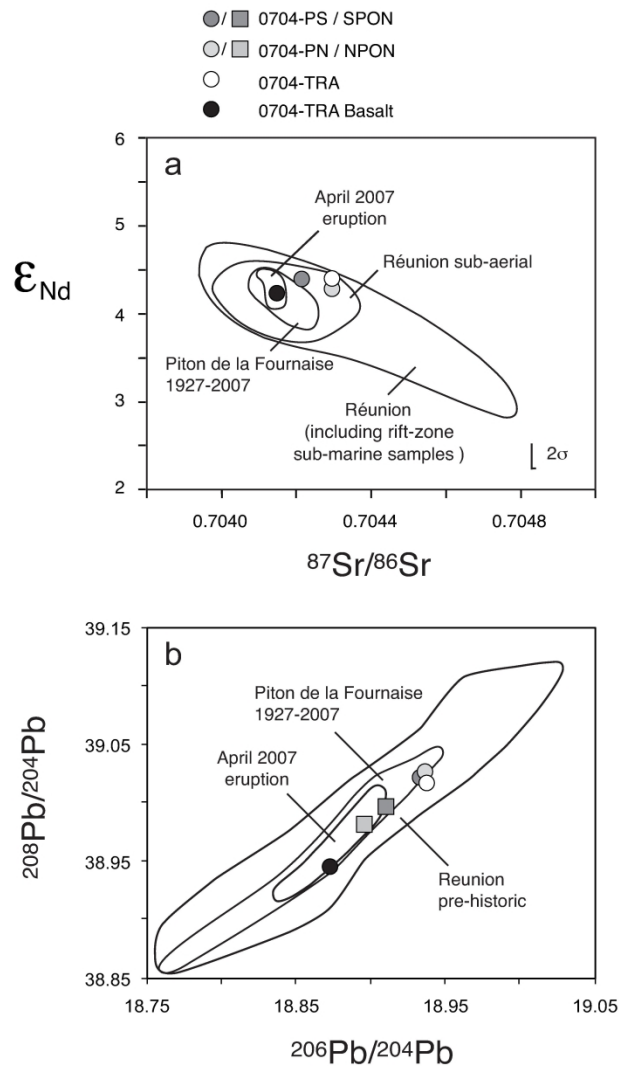
F4



Trace element patterns of the April 2007 trachytic pumice and the basaltic coating. Concentrations are normalized to the average concentrations of steady-state basalts (SSB) given in Electronic Appendix 1. SSB are the dominant homogeneous basalts of La Réunion Island (Albarède et al., 1997). Pattern of 0704-PS is drawn using the data obtained with NH_4HF_2 dissolution. Pattern of 0704-PS is drawn combining data obtained with savillex (Li, Cs, Pb) and alkali fusion (other elements) dissolution methods. Pattern of 0704-TRA is the mean of analyses of chips #1-4 (savillex) with Zr-Hf data from chip#7 analysis (Parr 250°C). Vertical lines indicate elements with negative anomalies.

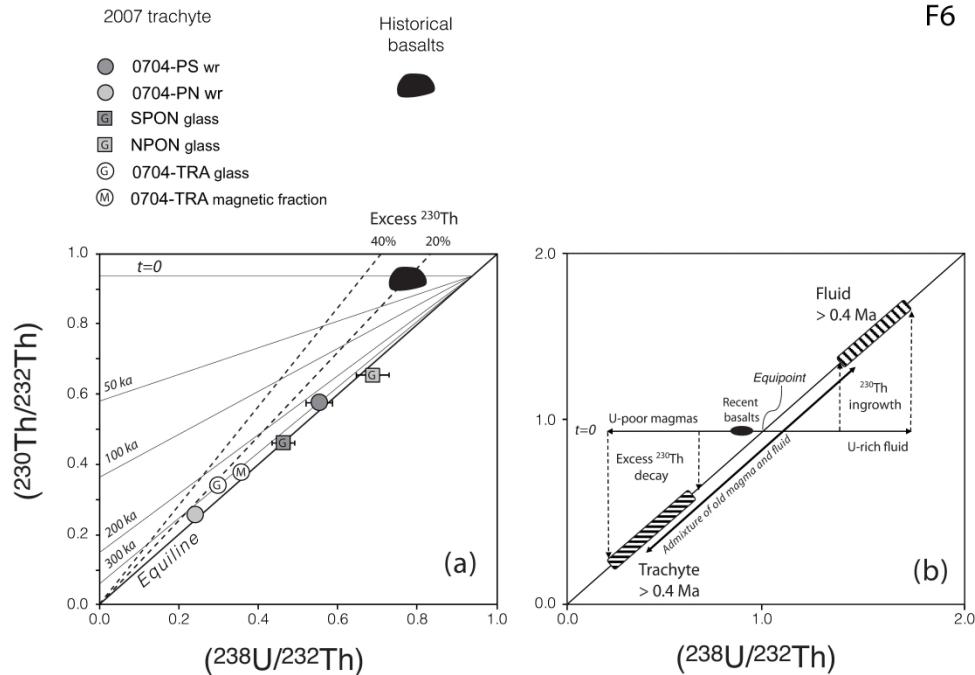
178x243mm (600 x 600 DPI)

F5



Sr-Nd-Pb isotope plots. The signature of the trachytic pumice and the basaltic coating is compared to that of La Réunion lavas in $^{143}Nd/^{144}Nd$ vs $^{87}Sr/^{86}Sr$ (a) and $^{208}Pb/^{204}Pb$ vs $^{206}Pb/^{204}Pb$ (b) spaces. The $^{143}Nd/^{144}Nd$ ratios are shown using the ϵ_{Nd} notation where $\epsilon_{Nd} = [(^{143}Nd/^{144}Nd)_{sample}/(^{143}Nd/^{144}Nd)_{CHUR} - 1] \cdot 10^4$ with $(^{143}Nd/^{144}Nd)_{CHUR} = 0.512638$. Error bars are shown in (a) and are within data symbols in (b). Data used to draw the La Réunion isotopic fields are from Fisk et al. (1988), Fretzdorff & Haase (2002), Bosch et al. (2008), Pietruszka et al. (2009), Smietana (2011), Vlastelic et al. (2005, 2007, 2009b, 2018).

150x236mm (600 x 600 DPI)



$(^{230}\text{Th}/^{232}\text{Th})$ versus $(^{238}\text{U}/^{232}\text{Th})$ isochron plot. (a) The composition of historical lavas of Piton de la Fournaise (black field) is drawn using the data of Sigmarrsson et al. (2005) and Pietruszka et al. (2009). Errors bars of $(^{230}\text{Th}/^{232}\text{Th})$ and $(^{238}\text{U}/^{232}\text{Th})$ are either shown or within symbol size. All but one trachyte samples plot within error on the equiline, which is indicative of ^{230}Th - ^{238}U radioactive equilibrium. Indicative isochrons are shown for different values of t , using the equation: $(^{230}\text{Th}/^{232}\text{Th}) = (^{230}\text{Th}/^{232}\text{Th})_0 \cdot e^{-\lambda^{230} \cdot t} + (^{238}\text{U}/^{232}\text{Th}) \cdot (1 - e^{-\lambda^{230} \cdot t})$ where t is the age of Th/U fractionation and λ^{230} is the decay constants for ^{230}Th .

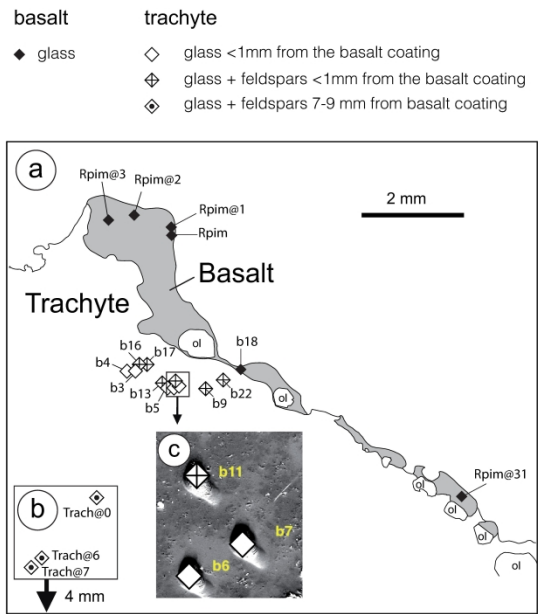
Dashed lines show 20% and 40% ^{230}Th -excesses, i.e. $(^{230}\text{Th}/^{238}\text{U}) = 1.2$ and 1.4 , respectively. (b) Schematic illustration of how the 2007 trachyte formed. Fractional crystallisation yields trachyte melt with identical $(^{230}\text{Th}/^{232}\text{Th})$ and $(^{238}\text{U}/^{232}\text{Th})$ as the parental basalt (assumed to be identical to the recent basalts). During final magma differentiation ($t=0$), exsolution of fluids in which U partitions, but not Th, yields U-poor trachyte melt (horizontal arrows) and important ^{238}U - ^{230}Th disequilibria. Both the ^{238}U -depleted trachyte and the ^{238}U -enriched fluid age and strive towards ^{238}U - ^{230}Th equilibrium (broken vertical arrows). Radioactive equilibrium is established after approximately 0.4 Ma with the U-depleted trachyte and the U-rich fluid having acquired a very low and very high $(^{230}\text{Th}/^{232}\text{Th})$, respectively. At any time, the residual melt and the fluid plot on an isochron, on each side of the equipoint. If the system remained closed, mixing between melt and fluid could explain the large variation of melt composition along the equiline (Fig. 6 a).

If the melt and the volatiles have remained as liquid and fluid phases since over 0.4 Ma, a special thermal regime is requested beneath Piton de la Fournaise. Alternatively, the trachyte crystallised as micro-syenite and the volatile phase as hydrous minerals both of which were defrosted by the primitive 2007 basalt. Both these possibilities are discussed in the text.

279x195mm (600 x 600 DPI)

1
2
3
4
5
6
7
8
9
10
11
12
13
14
15
16
17
18
19
20
21
22
23
24
25
26
27
28
29
30
31
32
33
34
35
36
37
38
39
40
41
42
43
44
45
46
47
48
49
50
51
52
53
54
55
56
57
58
59
60

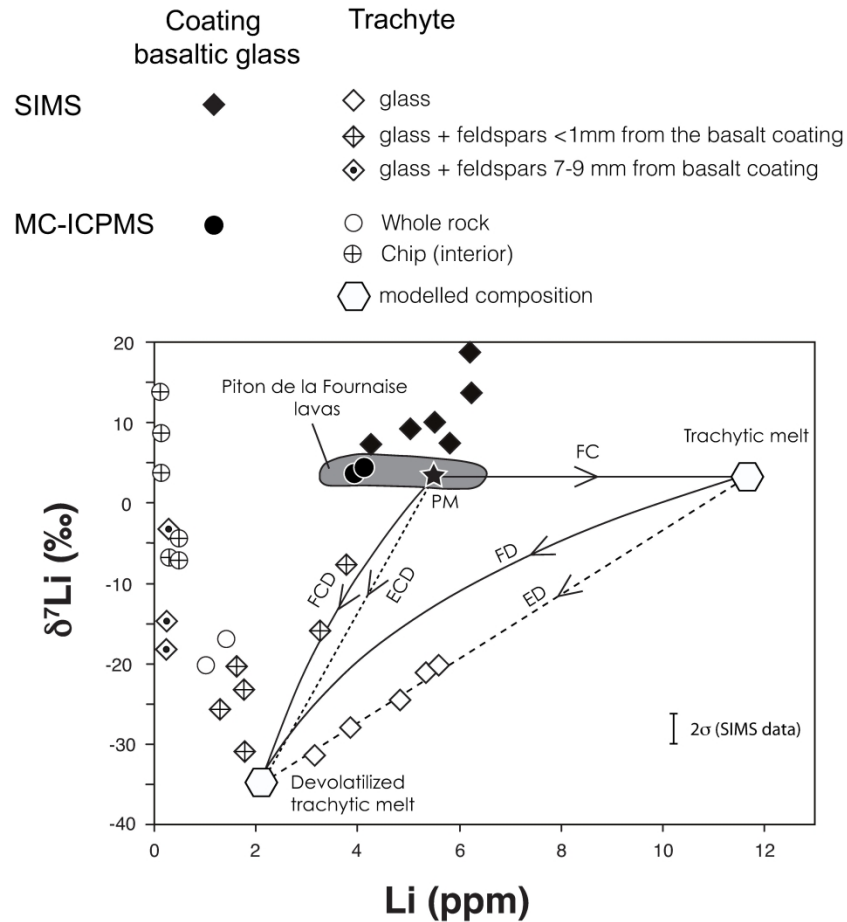
F7



Schematic cross section of sample 0704-TRA showing the loci of in situ Li isotope analyses. (a) Most analyses were done in the basalt coating (grey) and nearby in the trachyte (white). Ol: olivine crystals. (b) Three analyses were done in the interior of the pumice, 7-9 mm from the basalt coating. (c) Example of a SEM image acquired after SIMS measurements. These images were used to distinguish analyses performed on pure trachytic glass (light colour) from those done on glassy regions with abundant sub-micrometric K-feldspars (dark colour).

197x371mm (600 x 600 DPI)

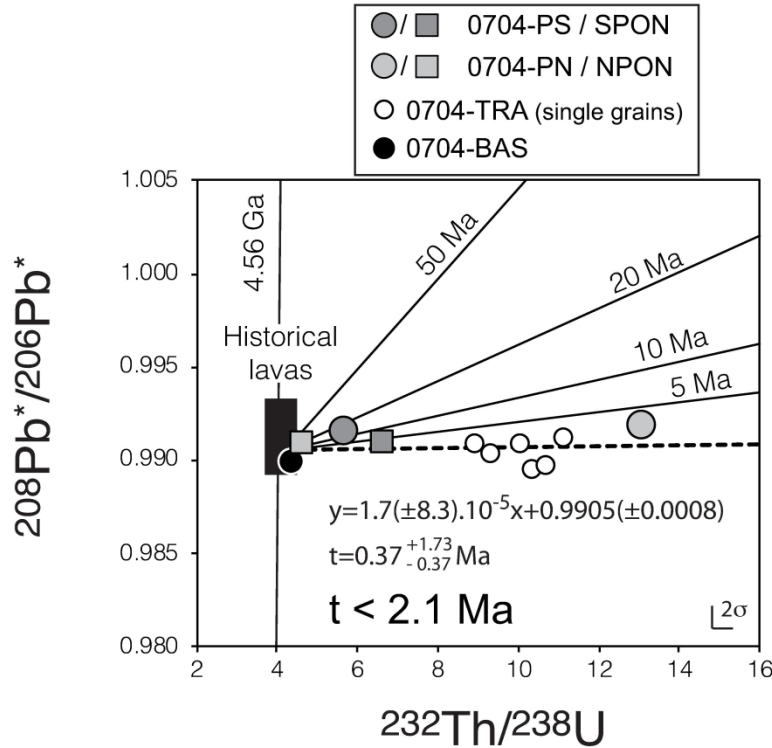
F8



45 $\delta^7\text{Li}$ versus Li concentration plot. Degassing and crystallization of a primary melt with 5.5 ppm Li and $\delta^7\text{Li} = +3.5\text{‰}$ (star labelled PM) is modelled considering four scenarios: Fractional Crystallization (FC) followed by Fractional Degassing (FD) or Equilibrium degassing (ED); simultaneous crystallization and degassing in an open system (FCD) or closed system (ECD). Depending on the crystallization-degassing scenario, the target composition of the devolatilized trachyte (Li = 2 ppm and $\delta^7\text{Li} = -35\text{‰}$) requires $D^{\text{V-M}}$ between 37 and 260 and $\alpha^{\text{V-M}}$ between 1.022 and 1.053. Only the FC-ED scenario with $D^{\text{V-M}} = 104$ and $\alpha^{\text{V-M}} = 1.048$ reproduces the linear array shown by the trachyte glass data (white diamonds). See text for detailed description of the model and related equations and assumptions. The field of Piton de la Fournaise (dark grey) is drawn using the data of Vlastelic et al. (2011).

189x273mm (600 x 600 DPI)

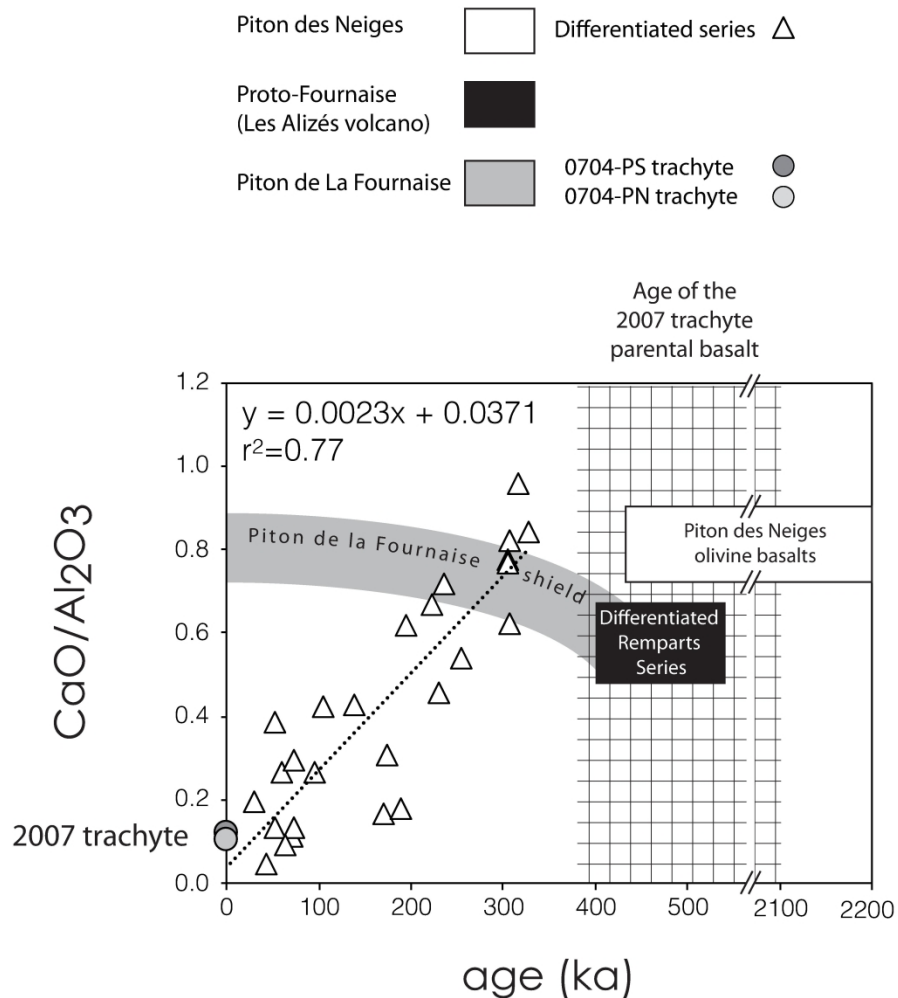
F9



$^{208}\text{Pb}^*/^{206}\text{Pb}^*$ versus $^{232}\text{Th}/^{238}\text{U}$ isochron plot. $^{208}\text{Pb}^*/^{206}\text{Pb}^* = [(^{208}\text{Pb}/^{204}\text{Pb})_S - (^{208}\text{Pb}/^{204}\text{Pb})_{\text{CD}}] / [(^{206}\text{Pb}/^{204}\text{Pb})_S - (^{206}\text{Pb}/^{204}\text{Pb})_{\text{CD}}]$ where subscripts S and CD refer to sample and Canyon Diablo meteorite, respectively. $(^{208}\text{Pb}/^{204}\text{Pb})_{\text{CD}} = 29.476$ and $(^{206}\text{Pb}/^{204}\text{Pb})_{\text{CD}} = 9.307$ (Tatsumoto et al., 1973). The slope-age relationship in this isochron diagram is given by: $^{208}\text{Pb}^*/^{206}\text{Pb}^* = [\kappa_1\mu_1(e^{\lambda^{232}\text{T}} - e^{\lambda^{232}\text{t}}) + \kappa_2\mu_2(e^{\lambda^{232}\text{t}} - 1)] / [\mu_1(e^{\lambda^{238}\text{T}} - e^{\lambda^{238}\text{t}}) + \mu_2(e^{\lambda^{238}\text{t}} - 1)]$ where $T = 4.56$ Ga, t is the age of Th/U fractionation, and λ^{232} and λ^{238} are the decay constants for ^{232}Th and ^{238}U . κ and μ are the $^{232}\text{Th}/^{238}\text{U}$ and $^{238}\text{U}/^{204}\text{Pb}$ atomic ratios, respectively. Subscripts 1 and 2 are relative to the intervals 4.56 Ga - t and t - 0 Ga, respectively. Indicative isochrons are shown for t in the range of 5 Ma - 4.56 Ga (plain lines). The regression line through trachyte data (dashed line) constrains Th/U fractionation to be younger than 2.1 Ma.

178x180mm (600 x 600 DPI)

F10



Temporal compositional evolution of La Réunion Island volcanoes. The CaO/Al₂O₃ ratio is used as a proxy for magma differentiation. Regression line through Piton des Neiges differentiated series (white triangles) is shown, whereas only temporal trends are shown for Piton des Neiges and Piton de la Fournaise shield stages because major elements and ages were not measured on same samples. The age estimated for the parental basalt of the 2007 trachyte is indicated (hatched area). The 2007 trachyte plots on the temporal compositional trend of the Piton des Neiges differentiated series, suggesting it could be a liquid remnant of the extinct volcano. Data source: McDougall (1971), Oversby (1972), Upton & Wadsworth (1972), Gillot & Nativel (1982), Albarède et al. (1997), Valer et al. (2017a).

186x245mm (600 x 600 DPI)